

<b>Title</b>	Solution processable metal oxide thin film deposition and material growth for electronic and photonic devices
<b>Author(s)</b>	Glynn, Colm; O'Dwyer, Colm
<b>Publication date</b>	2016-12-27
<b>Original citation</b>	Colm, G. and Colm, O. D. (2017) 'Solution Processable Metal Oxide Thin Film Deposition and Material Growth for Electronic and Photonic Devices', <i>Advanced Materials Interfaces</i> , 4(2), 1600610 (36 pp). doi: 10.1002/admi.201600610
<b>Type of publication</b>	Article (peer-reviewed)
<b>Link to publisher's version</b>	<a href="http://onlinelibrary.wiley.com/doi/10.1002/admi.201600610/abstract">http://onlinelibrary.wiley.com/doi/10.1002/admi.201600610/abstract</a> <a href="http://dx.doi.org/10.1002/admi.201600610">http://dx.doi.org/10.1002/admi.201600610</a> Access to the full text of the published version may require a subscription.
<b>Rights</b>	© 2016 WILEY-VCH Verlag GmbH & Co. KGaA, Weinheim. This is the peer reviewed version of the following article: C. Glynn, C. O'Dwyer, <i>Adv. Mater. Interfaces</i> 2017, 4, 1600610, which has been published in final form at <a href="https://doi.org/10.1002/admi.201600610">https://doi.org/10.1002/admi.201600610</a> . This article may be used for non-commercial purposes in accordance with Wiley Terms and Conditions for Self-Archiving.
<b>Item downloaded from</b>	<a href="http://hdl.handle.net/10468/6046">http://hdl.handle.net/10468/6046</a>

Downloaded on 2019-01-07T05:36:41Z

# **Solution Processable Metal Oxide Thin Film Deposition and Material Growth for Electronic and Photonic Devices**

Colm Glynn and Colm O'Dwyer\*

*Department of Chemistry, University College Cork, Cork, T12 YN60, Ireland*

*Micro-Nano Systems Centre, Tyndall National Institute, Lee Maltings, Cork, T12 R5CP, Ireland*

## **Abstract**

A comprehensive review of recent advances in solution processing and growth of metal-oxide thin films for electronic and photonic devices is presented, with specific focus on precise solution-based technological coatings for electronics and optics, and new concepts for oxide material growth for electrochemical, catalytic, energy storage and conversion systems, information technology, semiconductor device processing and related devices. Throughout, the nature of the soluble precursors solutions and their relationship to film formation process by various solution coating techniques are collated and compared, and highlight advantages in precursor design for creating complex oxides for devices. Because of the versatility of solution-processable oxides and functional material coating, it is important to capture the advances made in oxide deposition for plastic electronics, see-through and wearable devices, and high-fidelity thin film transistors on curved or flexible displays. Solution processing, even for oxides, allows control over composition, thickness, optical constants, porosity, doping, tunable optical absorbance/transmission, band structure engineering, 3D-substrate

coating, complex composite oxide formation and multi-layered oxide systems that are more difficult to achieve using CVD or ALD processes. We also discuss limitations of solution processing for some technologies and comment on the future of solution-based processing of metal-oxide materials for electronics, photonics and other technologies.

\* Email: [c.odwyer@ucc.ie](mailto:c.odwyer@ucc.ie); Tel: +353 (0)21 4902732; Fax: +353 (02)4274097

## 1 Introduction

A metal oxide thin film is composed of a deposit of material with a continuous and defined thickness over a specific surface. The thickness can range from single atomic or molecular layers to nanometres (nm) over many microns ( $\mu\text{m}$ ) depending upon the desired application. Modern devices and technologies incorporating metal oxide thin films rely on new and improved methods for their deposition.<sup>[1-2]</sup> Modern thin film device architectures and materials are investigated each year resulting in an associated increase in the range of applications available.<sup>[3]</sup> The growth in the need for metal oxide thin films in applications is reliant on cost-effective large scale deposition. The deposition of thin films for intricate devices, such as those in the semiconductor industry, has traditionally been performed using sputtering and evaporation methods coupled with solution processed techniques such as electrodeposition and etching methods. Solution processed thin films growth, where thin films are deposited from a precursor solution using a range of liquid deposition methods, are commonly used in the semiconducting industry for the deposition of resists.<sup>[4]</sup> The application of solution processed methods for the deposition of large-scale thin film in electrical and optoelectronic devices is becoming more important with the advent of flexible, stretchable, curved and plastic electronics and displays.<sup>[1-3, 5-6]</sup>

In applications requiring precise device architectures in three dimensions, as in most CMOS and related technologies, the use of solution processed techniques may not be competitive with respect to the current top-down lithographic based processes. In contrast, many emerging technologies that uses non-standard substrates that are curved, shaped, stretchable and made from materials that are extremely sensitive to heating steps, require thin film coatings with high surface uniformity and controllable morphologies over large areas, and this is where advanced solution processed techniques excel. The large scale deposition of uniform thin films is useful in particular for many applications including thin film transistors

(TFT's),<sup>[7-10]</sup> photovoltaics<sup>[11-13]</sup> and optical coatings to name a few, but there are many technologies that may benefit from advances in uniform large area coating of active materials on any type or any shape of surface.<sup>[14]</sup> An infographic on the various steps involved in depositing solution processed thin films is presented in Figure 1.

In order to produce thin films using solution processed techniques, a suitable liquid precursor must first be chosen and synthesised. These liquid precursors can be prepared using a variety of methods, from complex synthesis techniques to facile solution mixtures. Many types of precursors are possible, ranging from alkoxide/carboxylate derivatives<sup>[15-16]</sup>, sol-gel mixtures<sup>[17-18]</sup> to metallo-organic complexes.<sup>[1]</sup> It is important that both the chosen precursor solution and deposition method complement each other; the precursor solution can determine the most suitable deposition method. The reverse scenario is also true, where the chosen deposition method determines the best precursor solution and the nature of the chemical conversion and physical wetting of the surface. To complement the large variety of different liquid precursors, there are many different solution processed deposition methods available. These deposition methods each have their own benefits and drawbacks, particularly when depositing on different substrates with varied morphologies and surface energies.

Further integration of solution processed thin film technologies for large-scale applications depends upon the range of thin film materials and morphologies that can be deposited. To determine the thin films composition, crystal structure, morphology and electronic/optical properties, a large variety of different analysis methods can be used.<sup>[1, 15, 19-20]</sup> The focus of this review is to provide a thorough examination of the recent advances in solution based methods for oxide thin films, and functional film depositions using arrays and assemblies of nanoscale oxides, developed primarily for applications ranging from electronics and optoelectronics. We also compare and contrast the solution-based coating methods used for precursor and nanomaterial deposition into functional coatings and from a

detailed and critical examination of the recent literature, we summarise and correlate the device performance and properties to the coating methods and metal oxide precursors in a wide range of applications.

## **1.1 Thin Film Technologies**

Metal oxide thin films are used in a wide range of applications due to the range of different materials available.<sup>[1-2]</sup> Device architecture design can be employed to exploit different thin film material characteristics. The schematic in Figure 2 shows three possible uses of a conductive thin film material where the electrochemical, electrical or optical properties of the deposited material can be utilised for different applications. A material with favourable intercalative, electrical and optical properties, such as vanadium oxide (VO), can be used in a variety of applications as it provides numerous oxidation states and associated crystal phases.<sup>[21-23]</sup> For example, vanadium oxide (VO) materials can be paramagnetic, catalytic, electrochromic, thermoelectric, electronically conducting or insulating, and exhibit metal-insulator transitions at low temperature, simply by varying the oxidation state and crystalline phase. Electrical properties of thin film metal oxides can be exploited for their use in modern thin film transistor (TFT), CMOS technology and as dielectrics in the IC industry.<sup>[7, 24-26]</sup> The optical characteristics of many metal oxides are important for use in optical absorbing materials in solar cells, as transparent conducting oxides, as high mobility materials, or as antireflective or optical coatings.<sup>[14, 26-29]</sup>

Currently, an exciting area of research for thin film metal oxides concerns the utilisation of optical and electrical properties of a material in curved optoelectronic devices and in plastic electronics. Metal oxide thin films are used in both regular and polymeric/organic thin film photovoltaic devices, where they can be utilised as different

components within the devices: from the transparent conducting oxide (TCO) layer to the buffer/window and electron/hole transport layers.<sup>[12-13, 30-34]</sup> Other devices that use both the metal oxide's optical and electrical properties include electro/thermo-chromic materials,<sup>[35]</sup> self-cleaning surfaces,<sup>[14]</sup> sensors, optics and photo-electrochemical/catalytic devices for water splitting.<sup>[36-37]</sup>

The application of metal oxide thin films in modern technology and devices is an important avenue of research and while the advances in optical, electrical and physical properties of new oxides and comparison of overall device performance become more widely reported, it is important to classify the advances in metal oxide precursors design, their influence on the properties and choice of coating methods and the benefits of solution based processing for next-generation optoelectronic devices. Chemically designed precursors provide solution processable metal oxides that are compatible with semiconductor substrates, but also flexible plastic transparent substrates, but the processing conditions and properties compared to vacuum-based deposition are still under intense investigation so that they can exhibit tuneable optical transmission in different energy windows, and operate with (appropriately) high electronic mobility. If the precursor can be designed so that it can be solution coated over any type of surface and converted to a high mobility oxide phase with defined bandgap, and be electrochromic so that it has variable degrees of transparency at specific operating voltages in transistor form. A transistor-based device utilizing the above material would be a considerable advance for next generation displays and touch screens, light emitting devices, and also for tandem solar cells that operate in UV and infra-red wavelengths.

Metal oxides that are thermochromic and electrochromic should in principle provide optical transmission, but also optical filtering of unwanted wavelengths during operation; recent advances in solution processable high mobility oxides are only now being investigated

in device architectures to test the viability for such concepts. This work studies the various deposition and analysis techniques used for understanding the formation and characteristics of solution processed metal oxide thin films. Through fundamental thin film analysis both during and after deposition, coupled with methods to control the relationship between composition, growth and physical properties, the incorporation of thin films in modern technologies can be further improved.

## 1.2 Common Thin Film Deposition Techniques

There are many types of deposition methods available for metal oxide thin films, ranging from physical (PVD)<sup>[26, 38]</sup> and chemical (CVD)<sup>[39]</sup> vapour deposition, atomic layer deposition (ALD),<sup>[40]</sup> and solution deposited techniques.<sup>[1]</sup> The benefits and drawbacks for each of the deposition techniques can be discussed in terms of their cost, scalability, surface adhesion and coverage, the reproducibility of depositions (crystal structure, composition, phase) and the types of substrate upon which they can be grown.

The thin films produced from physical vapour techniques, namely those based on sputtering of a metal target both in vacuum and under a variety of gases, or indeed CVD processes involving the thermal decomposition and reaction of precursors, are known to have better control over the thickness and surface morphology of the thin films which have been the industry standard for semiconductor substrate-based technologies.<sup>[41]</sup> Physical vapour deposition techniques, such as magnetron sputtering as one example, can deposit crystalline thin films at low substrate temperatures.<sup>[26, 41-42]</sup> The crystallinity can be controlled by adjustment of the plasma energy of the sputtering system.<sup>[38]</sup>

Other methods of thin film deposition include ALD, which deposits a material by sequential atomic layer-on-layer growth by reaction of precursors at a surface.<sup>[43]</sup> Using ALD,



a very uniform thin film can be deposited on the surface of a substrate with precise control of the thickness. The drawbacks to the technique are mainly due to the high cost of the apparatus and the slow sample throughput due to the number of deposition steps involved in depositing a thin film with increased thickness. The primary drawback is the cost per layer for expensive precursors, and advancements in ALD rely on alternative precursor development. Further improvements on this technique can be obtained through the adoption of a vapour based technique and using atomic vapour deposition (AVD), which is commonly known as liquid injection vapour chemical vapour deposition (Li-CVD).<sup>[44]</sup> Overall, the transition to solution based methods is primarily driven by the need for lower temperatures and the coverage of non-transitional substrates.

## **2 Precursor Solutions: Design and Preparation for Solution-based Coating**

A multitude of bespoke chemical precursor solutions are now available for solution processed deposition techniques. In their simplest form, the solutions are prepared by mixing the metal oxide precursors with a suitable solvent to a known viscosity and composition. Various types of catalysts (materials that increase the effectiveness of the formation of the material via chemical reduction or inorganic compound decomposition) or inclusions (such as nanoparticles or fillers) may be added to the solution to give better control over the dissolution of the precursor with the solvent. Catalysts and inclusions can also be added for varying the solutions physical properties such as evaporation rate, viscosity, wetting characteristics or sheer-thinning etc. to suit the coating method. Precursors can range from simple metal oxide powders<sup>[45]</sup> and nitrates<sup>[46-47]</sup> and their mixtures, generally used in preparation of colloidal-like sol-gels, to liquid precursors containing metal oxide complexes encapsulated by organics, such as in alkoxide<sup>[48]</sup> and carboxylate<sup>[49]</sup> materials, which facilitate the formation of the deposit through formation reactions such as hydrolysis or

condensation processes. More complex systems involve macromolecular complexation of metal centres to form oxides via thermal or other forms of decomposition and oxide formation.

Figure 3 shows a general schematic of the typical steps involved in the formation of precursor solutions for a variety of solution processed techniques. In the case of alkoxide precursors, an anhydrous solvent, which is generally the parent solvent of the alkoxide, is added to help slow or limit the hydrolysis reaction, thus enabling sufficient time for deposition of the thin film.<sup>[50-52]</sup> The same technique can be used for the formation of carboxylate based precursors through solvent addition.

The preparation of sols from metal oxide powders and nitrates involves the dissolution of the material with a suitable solvent, with further stirring and heating often required. In preparing a Zr-incorporated aluminium oxide (ZAO) thin film, Jo *et al.* dissolved both aluminium nitrate nonahydrate and zirconium(IV) acetylacetonate in 2-Methoxyethanol (2-ME) at a variety of ratios and stirred for 12 h at 75 °C until the solution was clear.<sup>[53]</sup> The stirring and heating steps were required for a high quality precursor solution to be prepared. This type of sol preparation is common in the literature, both with and without heating or aging steps, and is now routinely adopted for forming materials composed of binary and ternary high field effect mobility metal oxides such as ZAO, IGZO etc.<sup>[46-47, 53-54]</sup> that are the mainstay of modern oxide electronics.

The use of additives in solution processed techniques is not a new practice, with many different roles found in the synthesis of liquid precursor solutions for a variety of additive materials, such as acids, catalysts and polymers. One of the benefits of additives for precursor solutions is to either increase the shelf life of the solution, or to decrease the length of time for the material formation. Sanchez *et al.* discusses the effects that different additives can have on the precursor solution, such as alterations to the gelation time and improving the long

term storage ability of the solution, which is beneficial because it increases lifetime and thus the number of depositions possible using a single batch of material.<sup>[52]</sup> Bhuiyan *et al.* discusses the use of modifying ligands, such as acetic acid or acetylacetone, which are used to chelate the alkoxides and thus reduce the sensitivity of the precursor solution to hydrolysis.<sup>[3]</sup> Bhuiyan *et al.* also describe how the nitrate method of precursor solution formation can be detrimental to thin film formation due to dewetting during deposition<sup>[3]</sup>, however, as can be found in the literature, the detrimental effect can be overcome through the use of an additives such as ammonia.<sup>[54]</sup> Solution processed methods can also enable doping techniques where dopants can be added to the precursor prior to deposition.<sup>[18]</sup>

Polymer assisted deposition (PAD), has been applied to materials research since Jia *et al.* published their first paper on the subject in 2004.<sup>[55]</sup> The application of PAD in solution processed techniques involves the use of polymers to stabilise the metal precursors and increase the uniformity of the deposited thin films.<sup>[1, 15, 55-57]</sup> PAD involves the incorporation of a polymer, originally PEI, into the solution through the formation of additive complexes and covalent complexes between the nitrogen atoms and the metal cation as outlined by Burrell *et al.*<sup>[56]</sup> The polymer stabilises the metal complexes so that they do not experience pre-formation in the solution prior to polymer decomposition,<sup>[56]</sup> thus increasing the lifetime of the solution and prevents early metal oxide formation during the deposition stage.

While the precursor that comprises two solutions may be the same, the mixture ratio of the individual components, alkoxide/solvent for example, is often altered for the specific purpose of the experiment. Chen *et al.* prepared a vanadium pentoxide ( $V_2O_5$ ) alkoxide precursor solution for forming thin films with an IPA-Alkoxide- $H_2O$  mixture ratio of 76-1-19,<sup>[12]</sup> whereas the same precursor solution is also used by others at different IPA-Alkoxide ratios of 9-1, 25-1 and 100-1.<sup>[15, 58-59]</sup> In each case, a  $V_2O_5$  thin film was formed from an

alkoxide precursor solution where a best-fit ratio can be chosen in order to attain desired deposit morphologies.

### **3 Deposition Techniques**

Choosing a precursor solution is only the first step in preparing a solution processed thin film material. As discussed, there are many different methods possible for depositing liquid precursors onto substrates to form a solid thin film. Each technique has its own advantages and disadvantages, which can depend on the chemical and adhesion attributes of the precursor solution and the substrate. Many publications<sup>[1, 24, 60-61]</sup> have previously described in detail the different types of techniques available, and here, highlights of some of the most popular methods are described together with a discussion on some of the latest innovations that have been introduced over the years. The scope of this section also includes the deposition of other materials through solution processed methods, as improvements to each technique can be applied to the deposition of metal oxide thin film materials. An overview of the process and notable examples of thin films deposited through spin/dip coating, spray pyrolysis and ink-jet printing deposition techniques and the solution control PAD methods are presented in this section. Several other solution processed techniques such as doctor blading,<sup>[62]</sup> roll-to-roll processing,<sup>[63-64]</sup> various printing methods<sup>[65-66]</sup> and innovative self-assembly techniques<sup>[67-69]</sup> are also available for thin film deposition.<sup>[1]</sup> The reader is directed to these references for further information on these techniques.

#### **3.1 Spin Coating**

Due to the well-understood processes governing thin film formation, spin coating continues to be one of the most popular deposition techniques for homogeneous layers both within

academia and industry. Figure 4 (a) illustrates the typical steps of the spin coating process. The precursor solution is deposited on the surface of the substrate which is held on top of a chuck within the spin coater. It is important that the solution covers the substrate surface completely prior to the spinning. The substrate is coated with solution and the spin coater accelerates rapidly to a high RPM and held at this speed for a set length of time. When the spinning is complete the thin film has been formed through a combination of liquid flow and evaporation processes. Depending on the type of precursor used the thin film may require some additional processing steps, such as heating or UV treatment, to be fully formed.

The processes involved in spin coating have undergone much experimentation and modelling so that the formation of thin films with specific as-deposited thicknesses can be formed. For most precursor solutions the as-deposited thickness of a thin film follows a general rule with regards to spin speed and duration. Figure 4 (b) shows a basic approximation of how changes in spin speed and duration effects film thickness; as both speed and duration increases there is an associated decrease in as-deposited thin film thickness.<sup>[3]</sup> For best results, experiments are performed on new precursor solutions to determine the range of acceleration/speed/duration values required in producing a variety of thin film as-deposited thicknesses.

The modelling of the processes involved in spin coating relies on fluid dynamics and surface interactions. The analysis of the technique is comprehensibly presented elsewhere for readers that are interested in the full detail.<sup>[1, 4, 70-71]</sup> By modelling a solution's characteristics such as viscosity, density, shear-thinning, and evaporation rates, to name a few parameters, a powerful relationship between spin-coating parameters and the as-deposited thickness of thin films has been demonstrated. Interestingly, the analysis can also be used to determine a cross-over point during the deposition at which the dominating process controlling the thin film thickness changes. The first of the two dominating forces that determine the film thickness is

the liquid flow, which can be altered by changing the acceleration and spin speed. The second dominating force is the evaporation of the precursor solution. For many of the materials discussed above in Section 2, the effect of evaporation would be largely due to the higher rate of evaporation compared to other solutions, particularly aqueous solutions. Figure 4 (c) is a plot of thickness versus time for an ethanol solution that undergoes acceleration to 2000 RPM in 1 s.<sup>[70]</sup> The analysis of Figure 4 (c) shows that the cross-over point is reached quickly at ~1.67 s, where after this point the thickness is dominated by evaporation effects. This analysis highlights the importance of choosing a valid ramp time, as a longer ramp time can force the cross-over point to occur during the acceleration, which could have detrimental effects on the control of uniformity and thickness of the thin film.

For complex metal oxide thin films formed from precursors that become chemically modified after exposure to water, air, heat etc., the spin coating process becomes significantly more complex. Most complex oxides grown as uniform thin films still rely on vacuum deposition methods, with atmospheric pressure CVD systems beginning to come online. While solution based chemistry can provide more complex composition mixtures for eventual coating, the nature of the sensitive spin coating parameters (wetting, evaporation, volume changes and solidification) that are dynamic and often non-linear – thus, control of spin coating requires new models that are specific to the precursor, or precursors with useful compositions that are designed to fit current spin coating knowledge to maintain predictability in uniformity. The availability, cost effectiveness and homogeneity of deposited thin films by spin coating within academic and industrial settings ensures its popularity as a solution-processed formation method.

### 3.2 Dip Coating for Fast, Uniform Oxide Thin Film Formation

The dip-coating deposition process continues to be popular for thin films deposited on large and irregularly shaped surfaces. While the technique does not see as widespread a use in the semiconductor industry as spin-coating does, in part due to the amount of precursor solution initially required in the reservoir, dip-coating provides an option for many forms of material coating in industrial and academic arenas. While the conceptual formation mechanism of thin films through dip-coating is well understood and characterised for many polymers, solutions and composite liquid-borne species, important research is still being conducted so that the specifics of the method can be further investigated and used for more efficient depositions. While the mechanism for thin film formation continues to be investigated, moving forward there is a large demand for dip-coating techniques in forming thin films with complex and varied surface morphologies by deterministic modifications to the deposition technique.

The experimental procedure for a normal dip-coating technique is shown in Figure 5 (a), where the substrate is immersed in a precursor solution and then drawn out at a controlled rate. As the substrate is removed from the solution, a liquid film forms which undergoes solvent evaporation leading to the formation of a solid thin film composed of the active agent within the precursor solution. This solid thin film can then be further processed through thermal treatments or other post-processing techniques to cause a chemical conversion to the final phase. Multiple and sequential deposition steps can be performed to prepare multi-layered thin film deposits, such as utilising staircase iterative depositions where each subsequent layer is thicker than the previous.<sup>[16]</sup> The thickness of the thin film is controlled primarily through changes of the withdrawal speed. However, there are also various methods available to alter the thickness such as precursor solution concentration, varying deposition temperature and by performing the dip coating at an angle, or under acceleration, as notable

examples. In all cases, a synergistic cause-effect scenario is setup, whereby an increase in concentration affects physical properties of the deposit.

In Figure 5 (b) a schematic produced by Brinker *et al.* shows the processes involved in thin film formation in a steady state regime.<sup>[17, 72]</sup> In a steady state regime the receding drying line velocity matches the withdrawal speed. Different forces interact during steady state dip coating for forming the solid thin films which are outlined in the schematic. The forces include viscous drag, gravity, inertial forces and meniscus/gradient surface tension.<sup>[17]</sup> Through experimental design and analysis it is possible to use knowledge of the precursor solution to model the resultant thin film thickness.

A model proposed by Landau *et al.* for the deposition of a liquid film on a surface outlines how the liquid thin film is controlled by balancing the viscosity and surface tension of the material such that a continuous liquid film is formed during a constant withdrawal speed.<sup>[73]</sup> Here, the liquid is the solubilised precursor solution, which subsequently undergoes chemical modification. The Landau-Levich model determines that the liquid height ( $h_0$ ) is controlled by the withdrawal speed ( $U_0$ ), viscosity ( $\eta$ ), liquid density ( $\rho$ ), gravity ( $g$ ) and surface tension ( $\gamma$ ) such that

$$h_0 = 0.94 \frac{(U_0 \eta)^{2/3}}{\sqrt{\gamma} \sqrt{\rho g}} \quad (\text{Eq. 1})$$

The solid thin film is then formed through evaporation, gelation and solidification of this liquid film. Therefore, by manipulating the thickness of the liquid film the resulting solid thin film can be controlled. While the Landau-Levich model can be used to model the thin film thickness of a material through the solutions properties, there are other processes that must be accounted for in order for a full understanding of the thin film material to be reliably formed, and while the parameters of the solution vary dynamically for some precursors due to



different rates of chemical change within the liquid coating, substrate surface energies and wetting need to be taken into consideration.

Figure 5 (c) shows the effect of withdrawal speed on the thickness for a variety of solution precursors. In this case, each of the solutions used ethanol as the solvent for a variety of silica and titania materials together with various acid/polymer additives for preparing the solid thin film.<sup>[74]</sup> The plot of thickness versus withdrawal speed highlights a reversal in the trend after a specific point where a higher deposition speed increases thin film thickness. Faustini *et al.* showed that this effect is due to a change in the processes that control thin film formation and solidification due to either capillary or draining forces that act on the liquid film.<sup>[74]</sup> They referred to the two stages as the capillary/evaporation and draining/evaporation regimes, with both regimes dominating the formation of the thin film at both low- and high-rate withdrawal speeds, respectively.

Figure 5 (d) shows the schematics for dip-coating in both the slow- and fast-rate regimes.<sup>[15]</sup> In the draining regime, fast-rate deposition where Landau-Levich model dominates, the capillary forces are negligible as the withdrawal speed is high enough to negate meniscus effects. The solution wets to the surface of the substrate and excess material is drained; during the draining step, evaporation occurs, which forms the solid thin film. In the capillary regime (slow rate deposition), the thin film forms during evaporation of the solution while it is being slowly withdrawn. The slow withdrawal results in capillary feeding from the surface tension of the solution. In this regime, the effects of viscosity and gravity coupled with the rate of evaporation influence the thickness of the thin film.<sup>[1]</sup> At intermediate withdrawal speeds a combination of capillary, draining and evaporation processes are involved, which dictate the thickness of the thin films. Faustini *et al.* also examined the effects of changes to the precursor concentration and solution temperature combined with alterations to the polymer aiding the deposition.<sup>[74]</sup>

For many dip-coating depositions an important issue must be accounted for when using many of the common precursor solutions, many of which are composed of mixtures of different components and precursors. When choosing a withdrawal rate for a new material, it is important to take into account the chemistry of the materials within the solution as large differences in the evaporation rate of different volatile additives can result in a varied formation at the drying line, where the evaporation occurs at the highest rate. When materials with different evaporation rates are mixed in a solution and dip-coated, a staggered and non-uniform film deposition can result. The staggered deposition occurs as one material evaporates prior to the other such as seen by Nishida *et al.* where a sharp gradient was found due to a greater water content near the drying line compared to the water content of the overall solution.<sup>[1, 75]</sup> When depositing from a solution composed of a mixture of different materials, it is important that the properties of each of the components, particularly those relating to evaporation and wetting ability, are accounted for when experimenting with the dip-coating procedure. For example, in a dip-coating solution composed of both relatively non-volatile H<sub>2</sub>O and a volatile solvent, such as IPA or EtOH, there can be preferential evaporation of the solvent prior to the full formation of the liquid film and subsequent solid thin film.<sup>[75-77]</sup>

The effect of a precursor's attributes on the formation of a dip-coated thin film is highlighted in Figure 6.<sup>[15]</sup> A precursor solution composed of IPA, vanadium triisopropoxide and H<sub>2</sub>O mixed by volume at 1000:10:1 was dip-coated onto a glass substrate at a fast-rate speed of 2.5 mm/s. Using the Landau-Levich model for fast-rate dip coating in the draining regime, the resulting thin film thickness can be calculated to be approximately 7-8 μm after evaporation of the solvent. However, the measured thicknesses for the V<sub>2</sub>O<sub>5</sub> thin films were <100 nm per layer as determined through microscopy analysis. It was found that the hydrolysis mechanism of the alkoxide based precursor allowed for the formation of sub-100

nm thin films within the draining regime.<sup>[15]</sup> The evaporation, hydrolysis and subsequent solidification of the deposited liquid film as shown in the optical images and schematic of Figure 6 highlight how these coupled processes enable the formation of uniform thickness thin films at a rapid deposition rate. The chemical processes involved in the formation of a solid thin film from a liquid precursor can be utilised for the improvement of thin film deposition efficiency.

Dip-coating technologies continue to be expanded with new research focused on improving the ability to dip-coat a variety of different surfaces with new thin film structures and morphologies. Improvements in dip-coating techniques are not confined to metal oxides but can be applied to many different types of materials. Figure 7 highlights a selection of the different techniques currently being examined, where changes to the dip-coating attributes, ranging from the speed, substrate changes and solution alterations, can result in changes to the resultant thin film materials. In most dip-coating applications, the withdrawal rate is kept constant. Faustini *et al.* instead deposited thin films of metal oxides with graded thickness and refractive indices by accelerating the withdrawal speed during deposition.<sup>[78]</sup> Through this acceleration deposition technique, thin films with a graded thickness index, or functionality gradient, were produced as shown in the schematic in Figure 7 (a).

Alterations to the precursor solutions, other than through chemical additives, can also cause changes to the thin films. Figure 7 (b) and (c) both show how alterations to the precursor solution can alter thin film structure or increase the efficiency of dip-coating thin films respectively. In Figure 7 (b) the schematic of an infusion withdrawal technique used by Ye *et al.* to deposit a thin film with a polarity gradient is shown.<sup>[79]</sup> The technique does not involve conventional dip-coating; instead the substrate is left in position while two solutions are mixed in the reservoir by pumping in the secondary solution. As the secondary solution is pumped in, the reservoir is also emptied, thus mimicking the effect of withdrawal in

conventional dip-coating. A new method for decreasing the amount of solution required while facilitating large-scale dip coating depositions was demonstrated by Ceratti *et al.* who supported a precursor solution on top of a non-miscible liquid as shown in Figure 7 (c).<sup>[80]</sup> This technique allows for the active precursor solution to coat the surface of the material as in conventional dip-coating techniques, while also decreasing the amount of precursor solution required, which is of particular importance for dip-coating of expensive materials.<sup>[80]</sup>

The final types of dip-coating modification discussed here involve changes to the substrate, either through mechanical or chemical means, to influence the type of thin film deposited. Angle-dependent dip-coating (ADDC) is a technique where the substrate is withdrawn at an angle rather than orthogonal to the precursor solution surface. When depositing at an angle, the thin film can be prepared at higher thickness with a lower number of sequential coatings required. Another benefit to the ADDC method is the ability to deposit thin films of the same material at different thickness on either side of the substrate. Figure 7 (d) shows how both deposition angle and withdrawal speed affect the thin film thickness on the top and bottom surface of ADDC deposited thin films of a set concentration of TiO<sub>2</sub>.<sup>[81]</sup> Through this technique, a thin film of the same material can be deposited on both sides of a substrate with different thicknesses which is of particular interest for optical filter technologies.<sup>[81]</sup>

The last technique discussed in this section describes how chemical patterning can be used to render different areas on the substrate either hydrophobic or hydrophilic; when the substrate is dip-coated the hydrophobic areas are coated while the hydrophilic surfaces remain free of deposit. As demonstrated by Wang *et al.* in Figure 7 (e), this technique can be applied to a variety of substrates to form complex and intricate materials on a variety of substrates, even those containing pillars and other non-planar morphologies.<sup>[82]</sup> The various innovative techniques highlighted in Figure 7 illustrate how the use of a dip-coating

technique continues to be of great importance to the thin film industry due to the large range of alterations which can be implemented to improve the deposition processes. For plastic electronics and systems that require complex oxide channel materials, dielectrics or indeed multilayer optical absorbers or coatings, selective precursors design and specifically chosen dip-coating methods may provide a highly reproducible and scalable method for large area coatings on many types and many shapes of next-generation substrates.

### **3.3 Complementary Deposition Techniques: Spray Pyrolysis and Ink-jet Printing**

As described in Figure 1, there are a number of other solution processed techniques that can be applied in developing metal oxide thin film materials. These include techniques such as ink-jet printing and spray pyrolysis, both of which involve the deposition of the material by passing the solution through an opening, either as a liquid or by first atomising, and then depositing, the material onto the substrate as a spray. Schematic representations for both spray pyrolysis and ink-jet printing<sup>[65]</sup> techniques are shown in Figure 8.

In the spray pyrolysis process, a spray of solution is directed at a substrate by first atomising the precursor solution. The atomising is accomplished through techniques ranging from simple air blasting to more advanced ultrasonic/electrostatic methods.<sup>[83-85]</sup> An important aspect of spray pyrolysis concerns the heating of the substrate during deposition, which aids in thin film crystallisation and surface cohesion. An unheated substrate can result in defective thin film depositions, often with cracks. For best results, it is advisable to adjust the substrate heating for each type of precursor solution until the desired morphology is deposited.<sup>[83]</sup> Many other deposition attributes must also be accounted for when using a spray pyrolysis technique. The chemical attributes of the precursor solution must be compatible with the atomiser otherwise the solution can cause blockages and other detrimental effects

which can both alter the deposition or cause machinery defects. To increase sample coverage, many spray pyrolysis devices incorporate a moveable stage to allow movement of the atomiser over the substrate. Spray pyrolysis continues to be upgraded and expanded for enabling the deposition of more complex depositions and materials, even transparent transistor technologies.<sup>[86]</sup> However, the technique has limitations and the thermal atomization step and subsequent condensation onto the substrate limit the spatial phase homogeneity and the crystallinity. Often films approaching the quality of epitaxial growth are required in electronic devices, with defined composition, crystal structures and thus electronic conductivity, mobility, band gap etc. Such films are difficult to realise using spray pyrolysis. On the other hand rapid deposition of, porous, random assemblies of large area nanomaterial coatings are possible.

Most applications of ink-jet printing pertain to books and other reading materials; there is currently a substantial drive in the deposition of functional materials using the same technique since its inception.<sup>[87-90]</sup> Ink-jet printing techniques can be applied to a wide variety of materials, where the limiting factor of the method relies upon the attributes of the precursor solution and its interactions with the print head and the substrate. The precursor solution must have a high enough surface tension so as not to leak uncontrollably while also having a sufficiently low viscosity to allow for transport through the printing nozzle when required.<sup>[88]</sup> As has become very clear in the literature, the ink quality is paramount for all ink-jet printing where uniformity is important. Figure 8 (b) shows two of the most common ink-jet printing techniques that are currently in use: in the top schematic the ink is deposited on-demand using an inducer so that droplets are selectively placed on the substrate, in the bottom schematic a continuous flow of material is fed through the nozzle and is electrostatically deflected away from the substrate into a collection tray when an area is not to be coated.<sup>[65]</sup> For depositing complex morphologies and arrays of material, the ink-jet

printing head can be positioned over the surface of the substrate similar to a conventional office printer. Using this technique it is possible to deposit a large variety of materials, however, the limiting factors involve the types of inks which can be prepared, their usability and the resolution of the printing head/stage. For the deposition of sub-micron patterns onto substrates, high performance ink-jet apparatus will be required.<sup>[90-91]</sup> Figure 8 (c, d) shows two examples of inkjet printed devices that benefit from the selective positioning of the material by this method. A high mobility zinc indium oxide (ZIO) transparent conducting thin film is shown in Figure 8 (c), which shows the capability of the ink-jet printing technique for large area depositions.<sup>[92]</sup> The smaller scale and site specific deposition of the ink-jet printing technique is highlighted in Figure 8 (d) where an  $\text{In}_2\text{O}_3$  semiconductor line is deposited for use in a TFT device.<sup>[54]</sup> Ink-jet printing is a useful technique for both large and small area depositions due to its versatility and low precursor solution wastage, and with massively parallel scalability possible similar to paper printing – such a method in the future may be invaluable to plastic electronics and see-through optoelectronic materials for transparent displays.

### **3.4 Solution Control Technique: Polymer Assisted Deposition**

The addition of additives and other materials into a precursor solution to aid in the formation of thin films during deposition is not a new practice. However, in the past number of years there has been an increased drive for the development of polymer-assisted deposition (PAD) techniques for improving the deposition and material characteristics of solution processed thin films. PAD processes can be applied to the deposition techniques discussed above through alterations of the precursor solution. The PAD process involves the mixture of a soluble polymer with the metal complex within the liquid precursor solution to increase the control of the solutions attributes, such as viscosity, reactivity and to increase the shelf life of

the material.<sup>[55-56]</sup> PAD can thus influence the morphology, compositional consistency, thickness and the density of defects (among other attributes) during thin film formation, by incorporation of a compatible polymer while depositing using currently employed solution processable techniques.

A schematic detailing two PAD processes for the deposition of TiO<sub>2</sub> using spin coating is shown in Figure 9 (a,b). In the Ti complex shown in Figure 9 (a), a titanium triscatecholate compound was bound to PEI through dissolving and mixing in DI water with subsequent purification.<sup>[55]</sup> The resulting Ti complex is a binding of the Ti to PEI as a catecholate complex, however, the concentration of Ti present was shown to be low. The concentration of Ti ions was increased using the method detailed in Figure 9 (b), where the Ti was instead directly bonded to PEIC and then purified using Amicon ultrafiltration.<sup>[55]</sup> Jia *et al.* discussed how the second method produced a much more stable Ti solution, particularly toward hydrolysis reactions.<sup>[55]</sup>

Strontium ions were also bound by Jia *et al.* to PEI for a PAD technique in an effort to replicate a high quality, important strontium titanate high-k dielectric material almost entirely formed by PVD, CVD and ALD processes currently. Figure 9 (c) shows how the strontium was bound to the PEI as an EDTA complex.<sup>[55]</sup> By mixing a solution with equal molarities of Ti bound to PEIC and strontium bound to PEI, an epitaxial thin film of SrTiO<sub>3</sub> was deposited through spin coating on an LaAlO<sub>3</sub> substrate. A HRTEM image displaying the epitaxial deposition of SrTiO<sub>3</sub> on LaAlO<sub>3</sub> is shown in Figure 9 (d). The PAD processes utilised by Jia *et al.* allowed for a single layer epitaxial deposition of SrTiO<sub>3</sub> on LaAlO<sub>3</sub> with a dielectric constant greater than 200 and a loss of <1% at 1 MHz which is comparable to thin film dielectrics deposited using pulsed laser deposition.<sup>[55, 93]</sup> The use of PAD techniques has improved considerably in recent times, with many studies showing the efficacy of PAD techniques particularly in the preparation of epitaxial metal oxide growth with the underlying



substrate.<sup>[56, 94]</sup> The PAD technique increases the scope of the solution processed depositions allowing for an increased range of materials and stoichiometric surfaces to be prepared. Utilising the capability of polymers to affect the morphological<sup>[15]</sup> or structural<sup>[57]</sup> aspects of a thin film can be utilised for the formation of novel surfaces through solution precursor alterations while retaining the use of standard deposition methods.

#### **4 Comparison of Thin Film Deposition for Vanadium Oxides**

In this section a comparison is made between a variety of solution processed vanadium oxide (VO) thin films. Vanadium oxide is chosen as a comparative material due to its prevalence in thin film applications and the large range of oxidative states and structures available such as  $V_2O_5$ ,  $VO_2$  and vanadium sesquioxide ( $V_2O_3$ ). Two branches of vanadium oxide families, such as  $V_nO_{2n-1}$  and  $V_nO_{2n+1}$ , provide an astonishing range of physical property differences based on the oxidation state and associated crystal space group. The morphologies and attributes of solution processed vanadium oxide discussed in this section are not exhaustive, but this section of the review provides an overview of the range of structures and thin films possible, and how various precursors, PAD processes, deposition methods and processing can affect the ultimate uniformity of the final functional oxide coating.

##### **4.1 Thin Film Composition and Structure**

The analysis of thin film composition and structure following a solution based deposition process are compared and examined by reference to diffraction, spectroscopy and microscopy characterization including, but not limited to; Raman scattering spectroscopy, X-ray diffraction and X-ray photoelectron spectroscopy techniques. The crystalline structure, composition or lattice vibrational characteristics for the resulting material for vanadium

oxides not only show the complexity and variability in the literature with respect to the fine detail of the deposition parameters, but help in understanding of the appropriate analytical methods for correlating the final phase to how the film forms its final phase.

A schematic of two layers of van der Waals bound bilayered molecular structures of  $V_2O_5$  is shown in Figure 10 (a), with the V atoms in grey and the O atoms in red.<sup>[95]</sup>  $V_2O_5$  is the most stable oxidation state of VO materials with a crystalline orthorhombic unit and a layered structure which is beneficial for use in applications utilising intercalation such as energy storage and via cation insert for modification of conductivity and optical absorption.<sup>[96-98]</sup>

The Raman scattering spectra for a dip-coated  $V_2O_5$  thin film on ITO substrates deposited by Alsawafta *et al.* is shown in Figure 10 (b), where the precursor solution was prepared from a mixture of vanadium oxytriisopropoxide, IPA and acetic acid.<sup>[58]</sup> The Raman scattering spectra in Figure 10 (b) shows the thin films in an as-deposited state prior to annealing where no distinct Raman modes indicative of orthorhombic  $V_2O_5$  are noted, but are subsequently observed after crystallization at 500 °C.<sup>[58]</sup>

The deposition of orthorhombic  $V_2O_5$  can be accomplished using a variety of different precursor solutions. In Figure 10 (c), Raman scattering spectra for  $V_2O_5$  thin films deposited by spin coating using three different types of precursor is presented after annealing at 450 °C. The solutions were prepared from metallorganic, organic and inorganic based precursors where the resultant thin films are labelled as VNA, VOSG and VISG, respectively in Figure 10 (c).<sup>[99]</sup> Raman spectra show the formation of orthorhombic  $V_2O_5$  occurs in each case with the evidence of characteristic vibrational peaks with only small discrepancies present. Shifts in the V=O bond located at 993  $cm^{-1}$ , 995  $cm^{-1}$  and 999  $cm^{-1}$  respectively for the VNA, VOSG and VISG thin films is indicative of small changes to the oxidative state; a larger Raman shift corresponds to increased amount of  $V^{5+}$ . The work by Sahana *et al.* demonstrates

how the use of different vanadium based precursors can be utilised for thin film deposition using identical techniques with the formation of compositionally pure  $V_2O_5$  thin film materials. This result is important for applications where thin films are desired within a technique but a specific precursor may be difficult to form in ideally soluble form, or decompose at temperatures that are incompatible with the substrate, for example.

Disorder within the thin films can contribute to the formation of unwanted or defected crystal structures. Different methods can be implemented which can decrease the level of disorder within the crystal structure. The Raman scattering spectra of orthorhombic  $V_2O_5$  thin films deposited through dip-coating of an alkoxide based precursor mixed with IPA- $H_2O$  (LCP, HCP) and IPA-PEG (LCP-peg, HCP-peg) at different concentrations is shown in Figure 10 (d).<sup>[15]</sup> The presence of extra vibrations was found at  $168\text{ cm}^{-1}$ ,  $845\text{ cm}^{-1}$ ,  $880\text{ cm}^{-1}$  and  $935\text{ cm}^{-1}$ . The extra vibrations are commonly seen in depositions of  $V_2O_5$  and are attributed to vanadyl-oxygen bond displacement which occurs during the formation of the orthorhombic crystal structure.<sup>[15, 100-103]</sup> Interestingly, in the Raman spectra shown in Figure 10 (d) the presence of the extra vibrations are not found in the thin film deposited using a low concentration precursor solution when poly(ethylene glycol) (PEG) was added. The addition of PEG to the precursor solution as a PAD technique halted the formation of the defects within the  $V_2O_5$  crystal structure. This finding demonstrated the functionality of the PAD technique for the formation of stoichiometric pure  $V_2O_5$  thin films by eliminating disorder within the film.<sup>[15]</sup>

The effect of changes to precursor molarity for  $V_2O_5$  thin films deposited onto amorphous glass surfaces through a spray pyrolysis technique at constant substrate temperature is shown in the XRD data of Figure 11 (a).<sup>[104]</sup> In each case there is a distinct (001) peak present while the number of reflections indexed to  $V_2O_5$  increases as the precursor concentration increases. Akl *et al.* ascribed the increased intensity of the peaks to grain

growth or an increase in the degree of crystallinity within the thin films as the concentration increased. The crystal size was analysed through Voigt profile analysis of the line broadening, which showed saturation at concentrations of 0.2 M, 0.3 M and 0.4 M and a sharp decrease in crystallite size for the low (0.1 M) and high (0.5 M) concentrations.<sup>[104]</sup> The saturation was linked to the concentrations being appropriate for crystal growth while the mobility of ions is insufficient at low concentration, but too fast at high concentrations, leading to agglomeration.<sup>[104]</sup>

Spray pyrolysis of  $V_2O_5$  thin films using a  $VCl_3/H_2O$  precursor prepared by Irani *et al.* shown in Figure 11 (b) demonstrates that the substrate temperature also plays a key role in the formation of different VO structures.<sup>[105]</sup> The XRD patterns in Figure 11 (c) demonstrates how precise annealing and atmosphere control can enable epitaxial growth of a range of VO phases other than the most stable phase which is  $V_2O_5$ .<sup>[95, 106-108]</sup>

Figure 12 (a) shows the XPS analysis of the V 2p core-level photoemission peak in the characterisation of different oxidative states of VO thin films including  $V_2O_5$ ,  $V_2O_3$  and  $VO_2$ .<sup>[95]</sup> The charge state of an individual atom can be determined as shown in Figure 12 (a), where an increase in the core level binding energy indicates an associated increase in the positive charge of the atom.<sup>[95]</sup> Through careful data analysis it is possible to determine the oxidative state and structure of a range of VO materials.

In Figure 12 (a, c) we compare  $V_2O_5$  thin films deposited through a variety of different techniques. Included in the XPS spectra is the O 1s core-level photoemission located in close proximity to the V 2p core-levels discussed above. The  $V_2O_5$  thin films studied by Cho *et al.* were deposited on ITO glasses through both a brush painting and spin coating technique from a vanadium (V) oxytriisopropoxide based precursor solution. In a brush painting deposition, the precursor solution is spread over the surface with a “brush” similar to screen printing. For both the brush and spin coating techniques the solutions were stated to

have been optimised for deposition.<sup>[109]</sup> A direct comparison of the V 2p and O 1s peaks can be made between the two resulting thin films and is shown in Figure 12 (b). For both types of depositions the V 2p<sub>1/2</sub> is an exact match while a small shift in the binding energy of 0.3 eV for the V 2p<sub>3/2</sub> and O 1s peaks is present.<sup>[109]</sup> The XPS analysis by Cho *et al.* demonstrates the possibility of preparing near-identical stoichiometric V<sub>2</sub>O<sub>5</sub> thin films using two different solution processed techniques where the active precursor material for the solution was identical. The interchangeability of the precursor material in different solution processed techniques is important for the transition of laboratory deposition methods to industrial sized practices.

Comparisons of the O 1s and V 2p peaks for V<sub>2</sub>O<sub>5</sub> thin films deposited using either a solution processed or evaporation technique is presented in Figure 12 (c).<sup>[110]</sup> The solution processed V<sub>2</sub>O<sub>5</sub> (sV<sub>2</sub>O<sub>5</sub>) thin film was deposited by Zilberberg *et al.* from an IPA/vanadium (V) oxytriisopropoxide precursor solution while the evaporated V<sub>2</sub>O<sub>5</sub> (eV<sub>2</sub>O<sub>5</sub>) thin films were deposited at an ultra-high vacuum. An evaporated V<sub>2</sub>O<sub>5</sub> thin film sample (cV<sub>2</sub>O<sub>5</sub>) was exposed to air prior to XPS analysis while the eV<sub>2</sub>O<sub>5</sub> was left under vacuum between the deposition and analysis. Analysis of the V 2p<sub>3/2</sub> peak shows small amounts of V<sup>4+</sup> present in the sV<sub>2</sub>O<sub>5</sub> and cV<sub>2</sub>O<sub>5</sub> thin films which is evidence that the presence of some VO<sub>2</sub> has formed within the thin films.<sup>[110]</sup> The analysis by Zilberberg *et al.* suggests that this formation of small amounts of VO<sub>2</sub> within the thin films is due to their exposure to ambient atmosphere which partially reduces the V<sup>5+</sup> to V<sup>4+</sup>.<sup>[110]</sup> This work highlighted the usability of solution processed techniques where the equivalent detrimental effects were experienced by both the solution processed and physical deposited thin films.

## 4.2 Surface Morphology and Uniformity from Solution-Based Coating

The surface morphology and lateral uniformity in coverage and structure is critical for electronic devices, preventing short circuits between conductive layers, and ensures consistent resistivity of the deposit. Thickness uniformity also ensures consistent optical absorbance across the surface and for flexible or curved substrate, local thickness variation may promote failure during extended flexure. Figure 13 shows a collection of AFM and SEM surface images of  $V_2O_5$  thin films using various solution processed deposition techniques. Costa *et al.* ink-jet printed the thin films in Figure 13 (a) by depositing a precursor solution prepared from a mixture of  $V_2O_5$  powder and hydrogen peroxide resulting in nanoparticle formation. The nanoparticles were suspended in water forming a stable colloidal solution.<sup>[111]</sup> This colloidal solution was deposited onto a flexible PET/ITO substrate and tested to determine surface coverage and the produced thin film morphology. Costa *et al.* observed through their AFM analysis<sup>[111]</sup> that the  $V_2O_5$  thin film did not show the presence of spherical particles, instead both the AFM and rugosity (roughness factor) measurements show the surface of the thin film was composed of a  $V_2O_5$  ribbon structure, a common morphology in  $V_2O_5$  materials.<sup>[112-114]</sup>

The dip-coated thin films shown in Figure 13 (b) were prepared by Gökdemir *et al.* using an inorganic ( $V_2O_5$  powder in  $H_2O_2$ ) and organic (vanadium (V) triisopropoxide in IPA) based precursor solution.<sup>[115]</sup> The inorganic solution was prepared similarly to the nanoparticles used in the inkjet printing discussed in Figure 13 (a): a  $V_2O_5$  powder was mixed with hydrogen peroxide and stirred to form a liquid sol. The organic based solution was prepared using vanadium (V) triisopropoxide mixed with an appropriate amount of IPA and acetic acid to form a liquid precursor solution. The thin films were dip-coated onto a variety of glass substrates including ITO coated glass at a withdrawal rate of 100 mm/min and then heated for 20 mins at 150 °C. The AFM images in Figure 13 (b) shows the formation of a

smooth granular  $V_2O_5$  thin film surface in both the inorganic and organic case, however, Gökdemir *et al.* discusses how the organic precursor route results in a thin film with a smoother more homogeneous surface morphology and a smaller grain size than the inorganic.<sup>[115]</sup> These types of changes in grain size and surface homogeneity are of importance for many material properties of thin films in particular the optical characteristics.

Pinholes, a common thin film defect, are seen in the AFM image of Figure 13 (c), which is an example of a spin-coated  $V_2O_5$  thin film prepared from an IPA-vanadium(V) oxytriisopropoxide solution.<sup>[116]</sup> Zilberberg *et al.* deposited the thin films on glass and ITO substrates at rotational speeds ranging from 3000 – 10000 rpm to produce controllable thicknesses between 10 – 45 nm.<sup>[116]</sup> The pinholes routinely form as a result of solution dewetting during the thin film formation stage.<sup>[16]</sup> The pinholes were not found to strongly influence the rms roughness, which was stated to be relatively low at 0.4 nm.<sup>[116]</sup> The formation characteristics of the pinholes in thin films of either polymers or metal oxides,<sup>[16, 117]</sup> is a commonly studied effect due in part to the deleterious effect of pinholes on electronic and optical properties. Two methods for alleviating the formation of pinhole defects in dip-coated  $V_2O_5$  thin films are shown in Figure 13 (d).<sup>[16]</sup> Pinholes formed on the surface of the as-deposited thin film were shown to be alleviated through the application of PAD, with the addition of PEG-400, and by altering the solvent/precursor concentration.

The effect of different molar concentrations on the morphology of  $V_2O_5$  thin films deposited using a spray pyrolysis technique is shown in Figure 13 (e). The thin films were deposited on glass substrates at a temperature of 250 °C through spray pyrolysis from a vanadium trichloride solution mixed with double distilled water at concentrations of 0.4 M and 0.1 M respectively.<sup>[118]</sup> The thin films show a distinct morphology change between the two concentrations, with the 0.4 M thin films having a higher rms roughness than the equivalent 0.1 M thin film of 25 nm and 8 nm, respectively. These thin films have a much

higher rms roughness compared to the others discussed in this section, however, the capabilities of large scale surface depositions with spray pyrolysis is higher than many of the alternative methods, particularly for use in energy storage<sup>[119]</sup> and optical applications.<sup>[83]</sup>

Using drop-casting techniques, large surface coverages of VOs can be achieved in a short time, albeit with a drawback in surface homogeneity. Figure 13 (f) shows SEM images of a drop-casted V<sub>2</sub>O<sub>5</sub> film both before (left) and after (right) a calcination process.<sup>[120]</sup> Lim *et al.* prepared the films by synthesising the rose-like particles with a sol-gel technique involving an ethanolic-aqueous medium, vanadium triisopropoxide and hexadecylamine combined with a long-term heat treatment technique. The prepared rose-like particles were suspended in ethanol and drop-casted onto Si wafers.<sup>[120]</sup> The SEM images in Figure 13 (f) show that a rougher surface after calcination is found. A high surface roughness can be a beneficial attribute for a variety of applications such as energy storage and in the case of these particular films, their use as a photoswitchable super-hydrophobic/hydrophilic material.<sup>[120]</sup>

### **4.3 Optical Properties of Solution Processed Vanadium Oxide Thin Films**

The study of a thin film's optical properties and characteristics is required for ascertaining the suitability of a material in optoelectronic applications, optical coatings and for assessing the nature of light-matter interactions for new materials and their arrangements. One of the most common techniques involves the calculation of the effective optical bandgap. The optical bandgap is the energy threshold for light absorption of the material and can be calculated through analysis of the absorption edge using the modified Davis-Mott relation and is commonly presented as Tauc plots for amorphous semiconducting materials or those that approximate such a condition.<sup>[121]</sup> The optical bandgap, threshold where optical absorption



can occur in the absence of scattering, can be calculated from the absorption coefficient through the relation  $\alpha h\nu = A(h\nu - E_g)^n$  where  $\alpha$  is the absorption coefficient of the thin films,  $A$  is a constant and  $E_g$  is the effective optical bandgap. The absorption coefficient determines the depth at which a given wavelength penetrates the material. The exponent  $n$  is related to the type of transition for the material. The optical bandgap can then be determined through extrapolation, where  $[\alpha h\nu]^n = 0$ . It is also possible to use the Moss relation to determine the refractive index from the calculated optical bandgap through  $n_{VO}^4 E_g \sim 95 \text{ eV}$ .<sup>[122-125]</sup>

For comparison to solution processed techniques, the UV-Vis spectroscopy in Figure 14 (a) shows  $V_2O_5$  thin films deposited by vacuum deposition at 3 nm (top) and 30 nm (bottom) thicknesses.<sup>[126]</sup> The UV-Vis spectra of the 30 nm and 3 nm thick layers of  $V_2O_5$  have a distinctive absorption edge at  $\sim 400 \text{ nm}$  with expected changes in the respected transmission values across the wavelength range.<sup>[126]</sup> Comparisons can be made with these vacuum deposited thin films to the transmission characteristics of equivalent solution processed  $V_2O_5$  thin films where changes in absolute transmission can be related to the effects of thickness while the optical bandgap shifts can be related to crystallisation and structural changes in the thin films.

The UV-Vis transmission and related Tauc plot (inset) shown in Figure 14 (b) are for the  $V_2O_5$  thin films deposited by spray pyrolysis. The deposits were prepared from pre-formed nanoparticles with a defined size, thus while the transmission increases at lower concentrations the optical bandgap remains consistent at  $2.44 \text{ eV}$ .<sup>[118]</sup> This optical bandgap value is higher than the range expected for bulk and nanocrystalline  $V_2O_5$  materials.<sup>[127]</sup>

Figure 14 (c) displays the UV-Vis transmission spectrum of the inorganic and organic thin films prepared by Gökdemir *et al.*<sup>[115]</sup> In comparison to the thin films of Figure 14 (b) a change in the absorption edge is seen in the transmission spectrum of Figure 14 (c). The

changes between an inorganic and organic precursor resulted in thin films with a calculated optical bandgap of 2.64 eV and 2.10 eV respectively when an  $n$  value corresponding to an indirect allowed transition is used. The changes in optical bandgap energy can be related to scattering and absorption caused by different constituent crystalline sizes within the films after crystallization of the precursors by the two deposition techniques.<sup>[115]</sup>

Post-processing techniques has an effect on the material characteristics of thin films. In Figure 14 (d, e) the changes which occur to the optical transmission of  $V_2O_5$  thin films using different post processing techniques is shown. Hancox *et al.* investigated the effect of deposition and annealing atmosphere on spin coated  $V_2O_x$  thin films in Figure 14 (d).<sup>[128]</sup> Thin films were spin coated under both ambient and  $N_2$  atmosphere followed by subsequent annealing in either of the two atmospheres. The optical images in Figure 14 (d) shows two examples each of thin films deposited under air (left) and  $N_2$  (right) respectively with both being annealed in air afterwards.<sup>[128]</sup> The effect of the  $N_2$  atmosphere during the deposition can be seen in the UV-Vis transmission spectrum where the  $N_2$  deposited (gold and blue) thin films have a higher transparency to the air deposited (green and blue) thin films.<sup>[128]</sup> The gold spectrum was both deposited and annealed in  $N_2$  while the green spectrum was deposited in air and annealed in  $N_2$ . Hancox *et al.* demonstrated that the deposition atmosphere had a larger effect on the optical properties of the  $V_2O_x$  thin films than the annealing atmosphere.<sup>[128]</sup> Post-processing  $O_2$  plasma treatment of spin coated  $V_2O_5$  thin films, as used by Bao *et al.* in Figure 14 (e), can be used as a low temperature method for crystallisation resulting in comparable UV-Vis transmission properties to thermally annealed thin films. Using this technique the  $V_2O_5$  thin films can be decomposed from the as-deposited amorphous material into the desired  $V_2O_5$  phase with no change to the optical bandgap.<sup>[129]</sup> The  $O_2$  plasma treatment allows for a low temperature post processing step which can be utilised for incorporation into polymer solar cells where high temperature processing can be

detrimental. Direct comparisons are made in Figure 14 (e) to both ITO, a common TCO, and PEDOT:PSS which  $V_2O_5$  can be used for replacing in polymer solar cells as a charge extraction layer.

By studying the optical characteristics of the  $V_2O_5$  thin films, comparisons can be made between the various deposition and post-processing techniques used for engineering the transparency and optoelectronic properties of thin films. As with the discussion on morphology alteration outlined above, the methods for altering the optical characteristics discussed are not an exhaustive list, however they do provide an overview of the types of changes that can be applied to help control  $V_2O_5$  thin film formation and be extended to many other transition metal oxides.

## **5 Thin Film Applications and Devices**

Metal oxide thin films have many applications within the optical, electronics, optoelectronics and energy storage/generation industries. The thin films are used as a variety of components within these devices, either as the working electrode/material, dielectric, hole/electron donor or as an optical coating for anti-reflection, filtering, or to increase/decrease hydrophobicity as a few examples. As outlined in previous sections in this review, there are many methods available for depositing these thin films ranging from evaporation and vapour techniques to the solution processed methods. The purpose of this section is to examine some of the latest developments in the use of solution processed techniques in preparing modern devices such as TFTs, photovoltaic cells, and battery materials, and for electronics and photonic devices. The devices discussed in this section are either fully solution processed or contain major components which have been deposited using one or more of the techniques outlined in Section 3. Section 5 presents examples of modern devices which incorporate solution

processed techniques in their fabrication. In many cases it is possible for the type of solution processed techniques to be interchanged for preparing thin film components, such as replacing a spin-coating process with dip-coating.

## 5.1 Solution Processed Electronic Materials and Oxides

The transistor is one of the fundamental building block devices for modern computing and electronics, and in display technologies.<sup>[2, 130]</sup> The continued improvement in transistor technology is driven by the need to make smaller and more energy efficient devices while also increasing the computing power.<sup>[131]</sup> The use of thin film transistors (TFTs) in fulfilling these needs is being intensively researched, due in part to the advent of curved displays, reduced size consumer electronics and peripherals, see-through electronics that rely on printed or coated organic semiconductors among other materials, and in flexible analogs of classical semiconducting device architectures.<sup>[132]</sup> The improvements required can be achieved by preparing TFTs that have a higher mobility, stability and uniformity. In the case of transparent TFTs a high level of optical transparency is also required. As outlined earlier, the deposition of active dielectric or channel materials for these devices in many cases relies upon expensive and time consuming processes. Using solution processed techniques, it is possible to cost-effectively form large scale assemblies of TFTs where each of the different components can be prepared sequentially, often on non-planar substrates.

In Figure 15 (a, b), Xu *et al.* developed TFTs using solution processed dielectric thin films, and by creating metal-insulator-metal (MIM) structures, they demonstrated that the frequency dependent capacitance of the  $\text{AlO}_x$ ,  $\text{ZrO}_x$ ,  $\text{YO}_x$  and  $\text{TiO}_x$  thin films had high values at low frequencies and low values at high frequencies.<sup>[133]</sup> Due to the low temperature

annealing, the  $\text{AlO}_x$ ,  $\text{ZrO}_x$ ,  $\text{YO}_x$  and  $\text{TiO}_x$  thin films exhibited an amorphous structure which limited the capability of determining the exact phase for each material.<sup>[133]</sup>

For high-k dielectrics the presence of defects and other non-uniformities influences the stability of the capacitance at different frequencies. As shown in Figure 15 (a) Xu *et al.* demonstrated a lower dispersion in the low frequency capacitance for  $\text{AlO}_x$  compared to  $\text{TiO}_x$  or  $\text{YO}_x$  dielectric thin films, which would indicate its suitability for use in a TFT. The explanation by Xu *et al.* stated that lower defect density and a smoother surface morphology for the  $\text{AlO}_x$  thin films contributed to the lower dispersion.<sup>[133]</sup> They also showed that processing  $\text{TiO}_x$  and  $\text{YO}_x$  dielectrics prevented breakdown and significant leakage current flow (Figure 15 (b)) up to electric fields of  $\sim 2$  MV/cm.<sup>[133]</sup>

In Figure 15 (c, d) the same dielectric thin films were used in TFTs with an  $\text{In}_2\text{O}_3$  semiconductor layer where the transfer and gate leakage characteristics were tested.<sup>[133]</sup> The behaviour of the  $\text{TiO}_x$  and  $\text{YO}_x$  dielectrics did not show suitability for the use in an efficient TFT device owing to leakage currents. The  $\text{ZrO}_x$  and  $\text{AlO}_x$  however showed a moderate and remarkable improvement respectively in their suitability as TFT dielectrics. The output characteristics of the  $\text{AlO}_x$  and  $\text{ZrO}_x$  are shown respectively for the  $\text{In}_2\text{O}_3$  TFT in Figure 15 (e, f) where a good ohmic contact is demonstrated without significant current crowding, at low source-drain voltage ( $V_{\text{DS}}$ ).<sup>[133]</sup>

The reproducibility of solution processed TFT designs was studied by Banger *et al.* who used a low temperature “sol-gel on chip” technique to prepare TFTs with the device architecture shown in Figure 16 (a).<sup>[134]</sup> The thin films were deposited using alkoxide based precursors that were spin-coated onto substrates in a cleanroom environment under controlled humidity. In Figure 16 (b,c), the mobility and turn on voltages for 49 identically deposited TFTs where Banger *et al.* showed that the solution processed TFTs had a similar performance with small deviations in both mobility and turn-on voltage.<sup>[134]</sup> While the reproducibility of

the technique would be less than that of the current large-scale deposition techniques such as physical vapour or CMOS technologies, it is at a level of reproducibility that highlights the possibilities of the sol-gel technique for active channel material deposition in TFTs.

The upscaling of TFT production using solution processed methods is under constant investigation.<sup>[1, 24, 134-135]</sup> The benefit of many solution processed methods is modularity of inorganic precursor solutions and the ability to apply them using a variety of coating methods whose degree of control is related to some parameter (spin rate, viscosity, wettability, evaporation, volatility, concentration, functionalization or dielectric constant, to name a few).<sup>[135]</sup>

In Figure 17, a novel bar-coating deposition method was used by Lee *et al.* to fabricate TFTs over a large area.<sup>[135]</sup> The bar-coating technique is schematically shown in Figure 17 (a) and involves the deposition of precursor solution onto a substrate placed in contact with the wired-bar rolling system. The wired-bar is moved horizontally at a constant rate while the interaction of the meniscus between the solution and bar results in the formation of a thin film. The final thin film material can then be thermally annealed to form the desired layer.<sup>[135]</sup> The bar-coating technique can be further enhanced through the application of self-assembled monolayers (SAM) which can encourage uniform surface morphologies to form, involving changes to the hydrophobicity of the underlying substrate or the roll bar. The impressive transfer and output characteristics of the bar-coated metal oxide TFTs shown in Figure 17 (b) have a high average field-effect mobility value of  $5.25 \text{ cm}^2 \text{ V}^{-1} \text{ s}^{-1}$ .<sup>[135]</sup> Interestingly, Lee *et al.* were able to compare the average mobility values of IGZO TFTs deposited through both a spin- and bar-coating technique. In Figure 17 (c), the IGZO TFTs formed through a bar-coating technique had a higher average mobility value than the corresponding spin-coated deposited TFTs from the same precursor solution. It was speculated that the longer evaporation time allowed in the bar-coating process resulted in an

increased thin film quality.<sup>[135]</sup> This improvement in the mobility values shows how the transition from a small- to large-scale deposition technique can have benefits with solution processed methods.

Different post-deposition processing techniques can be employed for treating as-deposited thin films to improve or alter many attributes of the thin films. These post-processing techniques can include thermal treatment/annealing at various temperatures and under different atmospheres, optical processing, curing or conversion using UV light, ozone decomposition/cleaning etc. and even chemical treatments to remove contaminants or other species from the surface. As with the different types of deposition techniques, the post-processing methods must also be chosen and tuned to the specific resultant thin films.

Yu *et al.* deposited  $\text{Cu}_x\text{O}$  thin films, where  $x$  defines the variation away from stoichiometric semiconducting  $\text{Cu}_2\text{O}$  affected by annealing conditions, through spin coating of a copper acetate monohydrate based precursor solution. The investigation<sup>[136]</sup> showed that, in Figure 18 (a), vacuum annealing (at  $2 \times 10^{-6}$  Torr and 200 °C) altered the thin film structure and composition such that the initial  $\text{CuO}$  thin film was reduced to  $\text{Cu}_2\text{O}$  at increased annealing temperatures. The oxide reducing mechanism in this case was attributed to phase boundary migration induced by oxygen out-diffusion along the moving phase boundary.<sup>[136-137]</sup> A  $\text{Cu}_x\text{O}$  TFT in Figure 18 (b) fabricated by the team, used a  $\text{Si}/\text{SiO}_2$  substrate and Ni source/drain electrodes. The transfer characteristics of the same  $\text{Cu}_x\text{O}$  TFTs vacuum annealed at different temperatures in Figure 18 (c) improved up to an annealing temperature of 600 °C. At annealing temperatures above 600 °C the transfer characteristics degraded. The improvement at 600 °C is attributed to the formation of  $\text{Cu}_2\text{O}$  and subsequent beneficial changes in crystallinity and morphology while the degradation at temperatures above this was due to detrimental island growth.<sup>[136]</sup> While the annealing temperatures used

may be too high for incorporation into current technologies, the role of the vacuum annealing can be studied for its effects at lower annealing temperatures.

One exciting and emerging technology currently under intense research is the formation of electronic devices on flexible substrates. These substrates allow for the incorporation of many different thin film devices within wearable and wear resistant applications such as wristwatches and e-paper displays. As with the incorporation of thin films into current devices and technologies, the application of solution processed methods in the formation of flexible electronics can be expected to be a driving force of research in the foreseeable future.<sup>[24, 138]</sup> The active interest in both flexible electronics and the variety of solution processed deposition techniques means that the two areas complement one another in their compatibilities.<sup>[24]</sup>

A solution processed device deposited on a polyimide (PI) substrate composed of IGZO/ZAO TFTs and circuits by Jo *et al.*<sup>[53]</sup> is displayed in Figure 19 (a). Initially a PI layer was spin-coated onto a glass slide with the IGZO and ZAO TFT devices and circuits deposited afterwards. The IGZO and ZAO thin films were deposited through spin-coating while the gate electrodes were prepared with sputtering. The thin films were deposited and subsequently protected with passivation layers which allowed the samples to be peeled from the glass substrate producing a flexible electronic device. Jo *et al.* also incorporated a deep ultraviolet (DUV) photo-annealing step in forming the channel and dielectric layers so that high temperature anneals were not be required. The typical transfer and output characteristics of the IGZO/ZAO TFTs is shown in Figure 19 (b, c) and displays high field effect mobility of  $\sim 11 \text{ cm}^2 \text{ V}^{-1} \text{ s}^{-1}$  with little to no hysteresis and a low gate leakage current. Interestingly, the electrical testing performed by Jo *et al.* demonstrated that the high field effect mobility was retained both before and after bending at a radius of  $R < 1 \text{ mm}$  showing the mechanical and electrical stability of the device.<sup>[53]</sup>



A comparison between the characteristic transfer and the saturation current mobility distributions of DUV photo- and thermally-annealed solution processed IGZO, IZO and  $\text{In}_2\text{O}_3$  semiconductor layers on an  $\text{Al}_2\text{O}_3$  gate dielectric with a source-drain voltage of 10 V is shown in Figure 20 (a).<sup>[138]</sup> Kim *et al.* demonstrated that the photo-annealed TFTs on glass substrates exhibited comparable or better electrical characteristics in relation to their thermally annealed counterparts. However, in order for the photo-annealing to facilitate these high-performance values, the photo-annealing stage must be performed in an inert atmosphere. In an inert atmosphere the photo-activation efficiency by the 184.9 nm emission does not undergo attenuation due to absorption of molecular oxygen.<sup>[138-139]</sup> In the presence of molecular oxygen the photo-activation efficiency is decreased resulting in poor thin film densification.<sup>[138]</sup> This photo-annealing method facilitated the formation of the flexible IGZO TFTs and circuits on a PAR polymer substrate seen in Figure 20 (b, c).<sup>[138]</sup> The formation of the seven ring oscillators (a common device for examples of new hardware constructed of an odd number of logic NOT gates where feedback is used to decide a true or false signal), shows the scalability of the technique enabled by the combination of solution processed deposition and low temperature DUV photo-annealing techniques which can be applied to both standard solid substrates and state-of-the-art flexible substrates.

## 5.2 Optoelectronic Devices and Solution Processed TCOs

In electronic applications, metal oxide thin films are a promising candidate in the future development of modern technologies. In the area of optical and optoelectronic devices the use of metal oxide thin film materials is already an industry standard. The application of solution processed methods into these industries is also commonplace, however they are generally used for large blanket coatings rather than conformal coating of intricate and often high aspect ratio device architectures that are common in modern optoelectronic devices. Solution

processed methods are not confined to metal oxide materials, particularly in optoelectronic and optical applications. Polymers, nitrides, sulfides and other oxides can also be deposited using these techniques which allows for a large diversity of device architectures to be made. The solution processed methods outlined in this section are commonly used with these other materials for depositing anti-reflection, self-cleaning, hydrophilic/phobic coatings and other such devices.<sup>[14, 61, 74, 140]</sup> The variety of applications in which solution processed layers of metal oxides are utilised are discussed in this section. In many of the cases each of the layers, including the metal oxide thin films, are deposited using solution processed techniques.

The use of transparent TFT devices is important as a key component in next-generation displays.<sup>[26, 86, 141-142]</sup> To achieve this, TFTs discussed in the previous section must be prepared over large areas using all transparent materials. Figure 21 (a) shows a schematic of a fully transparent TFT formed using ITO source/drain electrodes and a SnO<sub>2</sub> channel layer utilising ZrO<sub>2</sub> insulators.<sup>[143]</sup> Both the channel and insulator layers were deposited using a spin-coating process while the source and drain electrodes required a sputtering step. The transmission spectra and accompanying optical images in Figure 21 (b) illustrates the optical characteristics of the prepared TFT, which exhibited a high visible transmission. A high visible wavelength transparency is ideal for use in optoelectronic devices intended for displays as they can be integrated into devices without lowering the optical quality. Along with the beneficial optical properties, excellent electrical performances were found for the fully transparent thin films. The transfer characteristics in Figure 21 (c) show a high field effect mobility of  $\sim 90 \text{ cm}^2 \text{ V}^{-1} \text{ s}^{-1}$  possible without compromising a high transparency.<sup>[143]</sup> The transparent TFT area of research is expanding due to the desire for “invisible” circuits for applications in the optoelectronic sector with the cost-effectiveness of solution processed techniques cited for being a major contribution to the uptake of the technique.<sup>[86, 142]</sup>

The conductive channel layer is an integral component of many electronic and optoelectronic devices. The conductive layer must retain not only a high conductivity but a good field-effect mobility, and maintain a high transparency in the wavelength range of interest. Transparent conducting oxides (TCOs) are a range of metal oxide materials which fill this requirement. In Figure 22, the relative abundance of the different TCO compatible elements within the Earth's crust is shown. The lower the abundance, the higher the cost in their retrieval and thus the cost of the devices themselves.<sup>[144-146]</sup> There is a large drive in research to move away from Indium-based TCO materials and instead examine more affordable and abundant materials such as Titanium, Molybdenum, Zinc and Gallium that are not identified critical raw materials (CRM's). ITO remains the industry standard due to its well-documented deposition and device characteristics but advancements are being made with other materials.<sup>[147-151]</sup> Realistically, indium and other metal recovery is being made possible through green chemical routes.

While new TCO materials are being investigated, so too is the layer construction, where the morphology can vary from smooth TCO thin films to nanowire/dots assemblies and grids or arrays with defined porosity of an effective medium.<sup>[152-153]</sup> Two varieties of TCO architectures are shown in Figure 23, a planar deposition and a nanowire/thin film composite. The precursor concentration of the facile solution processed techniques were examined in both cases allowing TCOs with a range of conductivities to be deposited. Chen *et al.* deposited an ITO thin film with a high transparency comparable to the underlying glass substrate (Figure 23 (a)).<sup>[147]</sup> A high transparency is seen across the entire visible range with a decrease in the transmission shown at lower wavelengths due to the ITOs absorption edge.<sup>[147]</sup> The spin coated ITO thin films prepared by Chen *et al.* have a uniform surface morphology and thickness across a large area (inset Figure 23 (a)) where the percentage of Sn

within the solution can lead to fine control of the resistivity of the ITO thin film (Figure 23 (b)).<sup>[147]</sup>

A different type of TCO thin film was prepared by Chang *et al.* from a nanowire/film architecture (Figure 23 (c – e)) comprised of a layer of AgNWs deposited by the bar-coating technique and coated with MoO<sub>x</sub> by spin coating.<sup>[154]</sup> Using these two processes, they fabricated a highly conductive TCO over a large area, and importantly, demonstrated that this core-shell networked material assembly had better optical and electrical characteristics relevant to visible-frequency TCOs than either material alone. The aggregation of the MoO<sub>x</sub> coating around the AgNWs was postulated to lower the overall junction resistance, but they did not demonstrate any optimization of the density and spatial distribution of nanowire contacts nor a percolation threshold for this material system that is correlated to maximum network conductivity for a defined overall transmittance.<sup>[154]</sup> They did demonstrate for the networks examined, in Figure 23 (c), that the overall optical transmission of AgNWs treated with evaporated MoO<sub>x</sub> is marginally better, and was a function of the MoO<sub>x</sub> precursor concentration.<sup>[154]</sup>

As the MoO<sub>x</sub> precursor concentration was increased by Chang *et al.* the resistivity of the MoO<sub>x</sub> treated AgNW thin film decreases (Figure 23 (d)).<sup>[154]</sup> The changes in resistivity can be attributed to the MoO<sub>x</sub> coating the AgNWs where the SEM images of Figure 23 (e) demonstrated that rational changes to concentrations of the spin-coated MoO<sub>x</sub> resulted in thickness control of the resulting deposits around the AgNWs. This is important so that agglomeration that affects refractive index and inter-structure electronic contacts, that ultimately reduce optical transparency and electrical conductivity of the material network, is minimized. This strategy has a trade-off however for many such over-coated nanowire-based porous TCO layers, since the mechanical adhesion of the NW layer is reduced without the ‘binder’ coating, and adhesion is particularly important for flexible TCO technologies. The

optical images of Figure 23 (d) (vii) show how Chang *et al.* used this technique to coat a flexible polymer substrate while maintaining high conductivity and optical transparency with a high level of mechanical strength. After repeated tensile testing, consisting of 3000 bending cycles, the sheet resistance increased from ~30 Ohm/sq to only 43 Ohm/sq. For comparison, an ITO coated flexible substrate experienced an increase in the sheet resistance between 3 to 4 orders of magnitude higher after only 700 bending cycles, demonstrating the superior mechanical stability of the nanowire/film architecture deposited by Chang *et al.*<sup>[154]</sup> The use of carbon nanotube meshes are also under investigation for TCO preparation similar to the AgNW case.<sup>[153]</sup>

In an electrochromic (EC) material, light transmission can be reversibly modulated by the application of a voltage bias.<sup>[35, 155]</sup> The use of EC materials is very useful in green technologies such as smart windows, self-cleaning photocatalytic windows and self-adjustable electronic displays. The ability to control light absorption of windows within a modern building in an easily controllable way can decrease the level of cooling required through air-conditioning on warmer days. The EC mechanism involves the insertion and extraction of small ions, such as lithium for example, between a transparent conductor and EC material. In the case of an EC device, the ion is stored in a transparent film when not intercalated with the EC material.<sup>[35]</sup>

The periodic table in Figure 24 (a) highlights the various metals that in oxide form are capable of tunable optical transmission through EC processes.<sup>[35, 155]</sup> In an EC cathodic material, the switch from bleached to coloured states is achieved through ion insertion while an anodic material requires ion extraction. Vanadium based oxides<sup>[155]</sup> are excellent EC materials as they have been shown to operate in both anodic and cathodic regimes depending upon their oxidative state.<sup>[35]</sup> The density of available intercalation sites and the required cation diffusion distances within an EC material affects the optical contrast (change in

transparency between coloured and bleached states) and switching time respectively.<sup>[156-157]</sup> the method of coating of EC electrode films is critical in defining the areal consistency of oxidation state, thickness, absorbance, cation intercalation site availability and conductivity. In this regards, solution based deposition approaches are now being employed to coat non-planar EC electrode surfaces, making large area but uniform deposition important for next generation electrochromics.

An as example, Figure 24(b) shows an inkjet-printed VO thin film EC device where a number of transparency and colouring effects can be produced under cathodic and anodic voltage biasing related to lithium ion insertion/extraction to and from the VO material.<sup>[111]</sup> Previously Costa *et al.* also presented the same inkjet-printing method and characterisation technique for a tungsten oxide EC material with a remarkable colour contrast, particularly in the NIR region.<sup>[158]</sup> Different optical properties can be observed in Figure 24 (b) for a number of applied voltages in the VO thin films deposited by Costa *et al.* The corresponding pairs of oxidation and reduction peaks for each transition is shown in the cyclic voltammetry graph of Figure 24 (b) with the relevant Vis-NIR transmission spectra displayed in Figure 24 (c).<sup>[111]</sup> Costa *et al.* have demonstrated that changes in optical transparency are not limited to the visible wavelength range but also can affect the NIR spectral region, thus allowing EC devices capable of filtering thermal energy while transmitting visible wavelengths.

Other “green” thin film optoelectronic technologies under investigation are those which utilise light for energy generation. Many types of devices, architectures, and various energy generation processes exist, the mechanistic details of solar cells, photovoltaics and multiple-exciton generation etc. are outside the scope of this review. Instead, we look at some of the most recent advances in the application of solution processed thin film coatings for energy conversion and generation, namely in the areas of photo-catalysis and photovoltaics.

The use of photocatalytic processes in the splitting of water for the production of hydrogen as a fuel source has been under investigation for many years.<sup>[159]</sup> New techniques and methods in improving the efficiency are developed through increased research of photocatalysts, electrode materials and device architectures.<sup>[37, 160-162]</sup> Metal oxide coatings have been reported to increase the stability of semiconductors for long term photocatalytic processes<sup>[37, 161]</sup> with significant recent advances reported in the ability of TiO<sub>2</sub> thin films<sup>[160, 162-163]</sup> for stabilizing long term photo-electrochemistry. Thus far, ALD grown films have been the mainstay for highly uniform, thickness-controlled oxide deposits for water splitting and hydrogen evolution, but solution processed films may prove routes for electrodes with more complex shapes with uniform oxide coatings.

For improving the output of optical energy generation devices, researchers have begun to combining two types of devices that both harness energy from optical radiation in tandem structures. A common device architecture that uses this method are tandem solar cells, where multiple cells are layered on top of one another, each tuned to absorb different wavelengths, thus utilising more of the incoming radiation for efficient exciton generation.<sup>[164]</sup> However, recently there has been much research into the incorporation of different types of devices so that two modes of energy conversion can occur. The schematic for a combined photocatalytic and photovoltaic device is shown in Figure 25 (a), where both chemical and electrical energy are generated from the incoming photon radiation.<sup>[36]</sup>

In the device shown in Figure 25 (a), Abdi *et al.* combined an amorphous silicon solar cell with a gradient doped tungsten BiVO<sub>4</sub> photoanode using a cobalt-phosphate oxidation catalyst deposited through spray pyrolysis. The use of a common solar cell technology coupled with a state of the art photoanode and photocatalyst resulted in a device with a solar-hydrogen efficiency of 4.9% at a photocurrent of  $\sim 4 \text{ mA cm}^{-2}$ .<sup>[36]</sup> A novel aspect to the device deposition was the deposition method for forming the W:BiVO<sub>4</sub> electrode with a

graded doping profile. The state of the art electrode was deposited by altering the precursor concentration *in-situ* during the spray pyrolysis stage, providing an intriguing way of grading the doping profile without extrinsic processing. The use of the cobalt-phosphate oxidation catalyst also increased the photocurrent significantly, as can be seen in Figure 25 (b), and in both devices, solution processing was required not only for the material deposition, but also for rational control of the parameters that lead to enhanced efficiency from mutually cooperative device functionalities.<sup>[36]</sup>

The use of metal oxide thin films in photovoltaics is commonplace, with applications for different materials possible in each of the components, from the TCO to the active layer and charge extraction layers.<sup>[109, 146, 165-168]</sup> Yip *et al.* described how the use of all solution processed depositions and the incorporation of new materials and device architectures could theoretically increase the efficiency of single and tandem solar cells by ~10 % and ~15 % respectively over the next 10 years.<sup>[169]</sup> The charge extraction layer is required, particularly in polymer solar cells, where the extraction of the photo-generated charges needs to be facilitated.<sup>[110, 116]</sup> There are many options available for use as the charge extraction layer, notably PEDOT:PSS, however, in recent years many different high bandgap transition metal oxides have been investigated due to their more stable electrical characteristics. One of the most notable transition metal oxides examined for this application is V<sub>2</sub>O<sub>5</sub> with many publications on its efficacy.<sup>[12, 109, 166, 170-171]</sup>

The deposition of VO materials has previously been discussed in this review and demonstrates that V<sub>2</sub>O<sub>5</sub> can be deposited through a large range of techniques. Each of these methods can be adjusted and fine-tuned so that the desired thin film morphology can be deposited. The effect of either V<sub>2</sub>O<sub>5</sub> or PEDOT:PSS hole extraction layers on the power conversion efficiency of an organic solar cell under ambient conditions is shown in Figure 26 (a).<sup>[116]</sup> The data shows that a V<sub>2</sub>O<sub>5</sub> based device has an increased lifetime over an equivalent



PEDOT:PSS device which completely degraded after 400 h in air with no photovoltaic activity recorded after this time. This drop in efficiency was attributed to the degradation of the PEDOT:PSS layers over time while the  $V_2O_5$  layers were more robust with a longer life cycle. The power conversion efficiency for the  $V_2O_5$  charge extraction layers at different thickness in the same organic solar cells is shown in Figure 26 (b). The team discovered that the highest power conversion efficiency is possible at lower  $V_2O_5$  thicknesses. Zilberberg *et al.* postulated that at higher thicknesses, the increased optical absorption of the  $V_2O_5$  thin films in the absorption wavelength range of the P3HT active material decreased the efficiency of the devices.<sup>[116]</sup> When the thickness of the  $V_2O_5$  layer was too large, the benefit of the material in facilitating the extraction photo-generated charge carriers was compromised.

$MoO_x$  is another candidate as a charge extraction layer, and similarly to  $V_2O_5$  can be deposited using a variety of solution processed methods. In Figure 26 (c) an organic solar cell incorporating a  $MoO_x$  anode interfacial layer is depicted. A comparison was made by Yi *et al.* between a PAD solution processed  $MoO_x$  thin film to both evaporated  $MoO_x$  and PEDOT:PSS. The UV-Vis transparency of the different materials shows that the solution processed  $MoO_x$  has the highest transmission in the Vis-NIR range, and the highest photocurrent density of the three types of material they investigated.<sup>[172]</sup> This improvement in the PAD deposited  $MoO_x$  thin film compared to the evaporated thin film is attributed to the higher transparency at full surface coverage. The usability of solution processed methods in depositing uniform metal oxide thin films over large areas is of the utmost importance for their use in next-generation photovoltaic devices.

New transparent coatings continue to be researched due to the large number of applications that utilise thin films with UV-Vis to the NIR range absorption and transmission.<sup>[1, 14]</sup> Novel techniques for cost-effective deposition of transparent coatings are

under investigation, with one technique utilising inter-diffusion processes between a dip-coated vanadium oxide thin film and a glass substrate for the formation of a uniform transparent thin film shown in Figure 27.<sup>[125]</sup> Optical images and the accompanying UV-Vis-NIR transmission spectra of the initial as-deposited vanadium oxide thin film on glass and the same samples annealed at intermediate (250 °C) and high (300 °C) temperatures. The transparency of the thin films increase at the high annealing temperature to a value 90% – 97% of that of the underlying glass substrate due to interdiffusion processes. During the interdiffusion process, Si and Na species diffuse from the borosilicate glass substrate to the vanadium oxide layer resulting in the formation of a crystalline  $\alpha$ -NaVO<sub>3</sub> material surrounded by a glassy matrix, which the Raman scattering spectra in Figure 27 (c) detects. The schematic in Figure 27 (d) shows the interdiffusion processes between a deposited thin film and substrate and how the formation of the transparent coating effects the transmission and scattering of light. The interdiffusion between a solution processed thin film and a suitable substrate can result in the formation of optical coatings, invisible optical protection barriers and also as high-k dielectric materials, and possibly influence solution processed approaches for thin film doping.<sup>[125]</sup>

### **5.3 Miscellaneous Device Applications of Solution Processed Oxide Films**

As outlined in this review, significant developments have been demonstrated for solution processed metal oxide thin film deposition for a range of applications where optical, electronic, electrochemical and structural properties can not only be controlled in terms of uniformity and quality, but offer alternative methods for unique morphologies and compositions for a range of applications. The electronic and optoelectronic applications discussed above are some of the most common examples where solution processed methods are being applied. There are also a large number of other applications where niche uses are

being investigated. In this section, a brief overview of the use of solution processed methods in other thin film applications is discussed.

The use of metal oxide thin films in photocatalytic processes was discussed previously, however, their use in electrocatalytic devices is also important, and has received renewed interest in the last couple of years. In a water splitting electrocatalytic device, hydrogen and oxygen are produced through the electrolysis of water. A large factor for increasing their efficiency is through correct electrode and catalyst choice, as is also the case in many photocatalytic processes. The use of thin film electrocatalysts can have many benefits such as minimising the catalysts effect on overpotential due to their thinness, controllable film composition and morphology.<sup>[173]</sup> In Figure 28, different thin film electrocatalysts were prepared and their oxygen evolution reactions compared. Comparisons were made between the different materials with conditioned cyclic voltammetry measurements and Tafel measurements, showing that the  $\text{Ni}_{0.9}\text{Fe}_{0.1}\text{O}_x$  was a more efficient electrocatalyst than one of the best known electrocatalysts,  $\text{IrO}_2$ , for the types of measurements performed.<sup>[173]</sup> Interestingly, Trotochaud *et al.* were also able to show *in-situ* that the layered hydroxide/oxyhydroxide were the active catalyst through a structural transformation between oxide to hydroxide/oxyhydroxide.<sup>[173]</sup>

There are many types of sensors and sensing devices available, from thermal measurements using liquid cells to electronic sensors that monitor the electrical response of materials in different environments. Thin film sensors are particularly useful due to their small size and the range of materials available. The thin film sensor shown in Figure 29 (a) was composed of a spray deposited  $\text{V}_2\text{O}_5$  material prepared at different pyrolysis temperatures. The sensing response curve for the  $\text{V}_2\text{O}_5$  layers deposited at different temperatures was examined and shows that the highest response and thus most sensitive layer is that heated to 300 °C.<sup>[174]</sup> One of the factors that improved gas sensing responses of the

V<sub>2</sub>O<sub>5</sub> thin films deposited at 300 °C was the smaller material grain size. With a smaller grain size and an increase in surface area of the electrode, more of the surface is available for the sensing to occur and thus the sensitivity increases.<sup>[174]</sup> Possible methods for further improvement of the efficiencies may be the formation of mesoporous electrodes utilising the same materials but with greater surface areas through inverted opal morphologies.<sup>[175-176]</sup> Recent findings have shown that PAD processes and solution based V<sub>2</sub>O<sub>5</sub> coating uniformity is influence by the dynamic hydrolysis of nanoscale 2D flakes within the layered structure of the thin film, thus preventing dewetting and ensuring uniform crystallisation throughout the film upon conversion to the oxide during annealing.<sup>[16]</sup> Solution based methods offer a unique way of providing large scale uniform films that have nanoscale or mesoscale internal structure that is advantageous for some devices.

The incorporation of different VO's into sensing devices is commonplace due to the materials large range of oxidation states and its history as an industrial catalyst. The different VO materials can be used in a variety of sensors as either the main active material or for increasing the sensitivity, such as in the schematic shown in Figure 29 (d) where the V<sub>2</sub>O<sub>5</sub> is deposited on top of an amorphous silicon electrode to increase the sensitivity for ethanol detection.<sup>[114]</sup> The implementation and extended use of VO materials can be expected to continue for implementation with state of the art sensors and materials.<sup>[1, 177-179]</sup>

Solution processing methods are not limited to purely electrical or optical applications, but can also be applied to areas such as energy storage. In Figure 30 (a), a metal-oxide-semiconductor (MOS) device for use as a capacitor was created entirely by solution processed techniques. The SEM images in Figure 30 (a) show two different morphologies deposited using a dip-coating method on either glass or p-Si substrates.<sup>[180]</sup> The change in surface morphology is common in these types of depositions but can be adapted using many of the techniques discussed previously. The BiFeO<sub>3</sub> capacitors deposited by

Cetinkaya *et al.* showed stable insulation characteristics with a density interface states measurements equivalent to thin films deposited by sputtering.<sup>[180]</sup>

The electrochemical attributes of different materials are continually studied for integration into energy storage systems, electromechanical sensors and capacitors. A novel application for  $V_2O_5$  thin films is demonstrated in the schematic of Figure 30 (a) where standalone nanofiber sheet actuators were synthesised and tested as electrochemically modulated actuators.<sup>[181-182]</sup> The nanofiber sheet actuators were synthesised from a sol-gel mixture onto filter paper and subsequently peeled to produce the sheets. The resulting standalone layer of entangled  $V_2O_5$  nanofibers were tested by Gu *et al.* for electromechanical actuation by immersing in a LiCl aqueous electrolyte. Upon insertion and removal of the lithium into the  $V_2O_5$  through voltage sweeps the cantilever flexed either left or right as shown in the schematic. The mechanical stress experienced by the layer during flexing was analysed by Gu *et al.* using a sophisticated optical technique.<sup>[181]</sup> The generated stress and corresponding applied voltage is presented in Figure 30 (c). The structure of the  $V_2O_5$  material in this case showed a lower voltage requirement than other ferroelectric or electrostrictive materials, in part due to the ability of  $V_2O_5$  to insert Li-ions between the layers more easily, but the demonstrated proved an important point for solution processing of films capable of controlled mechanical deformation. Gu *et al.* theorised that the many uses and applications of  $V_2O_5$  would lead to the materials incorporation into multifunctional devices which would take advantage of their multifunctional properties, such as multicomponent sensors.<sup>[181]</sup> The research group led by Baughman have investigated many other materials utilising this effect for artificial muscle applications that also uses solution based approaches for functional material coating.<sup>[183-184]</sup>

The possible electrochemical responses of many metal oxide thin films imply that they are not limited to use in sensors and electronic or optics but can also be of great benefit

for battery technologies.<sup>[185-186]</sup> An ideal thin film battery would have a compact size while retaining high electrode surface area and a rapid charge/discharge cycle without capacity fade.<sup>[96, 187-188]</sup> These attributes can be obtained through the use and incorporation of flexible electrodes and substrates with thin film technologies. The capability of solution processed techniques in providing a battery with these capabilities while also allowing simpler doping (conductivity) and composition (chemical potential and cell voltage) control is an area under intense research.<sup>[62, 189]</sup> Pulverisation of the electrode during charge/discharge cycles caused by the stresses of insertion/removal of Li is a detrimental effect for Li-ion batteries, which tends to decrease the lifetime of devices. By wrapping and moulding the electrode and keeping the thin film to a low thickness a sufficiently high surface area can be formed. A thin film with sufficiently low thickness can accommodate the stresses caused by the insertion/removal of the Li ion in the direction away from the substrate or current collector, which can result in a high degree of reversibility in the cycle process.<sup>[97]</sup>

As an example, the ordered mesoporous  $\alpha$ -Fe<sub>2</sub>O<sub>3</sub> battery electrode shown in Figure 31 (a) was deposited from a liquid precursor through dip-coating onto various substrates such as FTO or p-Si and utilised a diblock copolymer to define the structure within the surface morphology.<sup>[190]</sup> The cyclic voltammetry and associated stored charge vs. sweep rate relationship for the  $\alpha$ -Fe<sub>2</sub>O<sub>3</sub> battery electrode is shown in Figure 31 (a), where the increased sweep rates limit the stored charge. The SEM images show that there is little large-scale degradation of the  $\alpha$ -Fe<sub>2</sub>O<sub>3</sub> thin films after 200 cycles of lithium insertion/removal.<sup>[190]</sup> The findings by Brezesinski *et al.* demonstrated that thin films of an inexpensive material such as  $\alpha$ -Fe<sub>2</sub>O<sub>3</sub> can be cost-effectively deposited using a di-block copolymer assisted solution processed technique and used to prepare a long lifetime Li-ion battery. In this example, the ability to create functional porosity and sub-structure in the active battery material, and the coating onto the electrode surface, were together possible by solution processing.

The preparation of a thin, flexible Li-ion paper battery is shown in Figure 31 (b – e) where the different layers are deposited through a doctor blade technique. A carbon nanotube film is used as a conductive layer while the battery electrodes consisted of either  $\text{Li}_4\text{Ti}_5\text{O}_{12}$  (LTO) or  $\text{LiCoO}_2$  (LCO) materials also deposited using the same doctor blade technique.<sup>[62]</sup> As demonstrated in Figure 31 (a) both the carbon nanotube and active materials are deposited onto a stainless steel substrate and then peeled off forming a free standing film. This free standing film is then laminated onto a paper substrate, Figure 31 (c), which is then prepared into a flexible thin film battery schematically shown in Figure 31 (d). An optical image of the final thin film battery is shown in Figure 31 (e). The final battery retained a capacity of  $\sim 110 \text{ mAhg}^{-1}$  after 20 cycles while no failure was observed after manual bending 50 times to 6 mm. The work by Hu *et al.* is a proof of concept for the realisation of an all solution processed flexible thin film battery for use in applications where embedded power devices are needed such as smartwatches, sensors and phones.<sup>[62]</sup>

## 6 Conclusions and Outlook

This review discussed and highlighted the advanced and growing importance of solution processable metal oxide thin films and structures for electronic and photonic devices, but also for a range of electrochemical, mechanical and catalytic systems. Specifically, solution processed techniques offer a wide range of possible deposition routes, ranging from the common spin-/dip-coating methods to the sophisticated printing and roll-to-roll depositions.<sup>[1-</sup>

<sup>2]</sup> Further development of these techniques will be required for industrial scale deposition required for next-generation applications that involve not only fully solution processable devices and active materials, but coating of patterned structures and non-planar, even flexible, materials.<sup>[2, 92, 146, 191]</sup> As detailed in this review, many of the precursors and deposition methods and parameters in solution processed techniques are interchangeable to

some degree, which facilitates scalability and flexibility in coating method, composition, and sequential deposition, ease of doping or modification of chemical, electrical and optical properties for example, and the comparative simplicity and accessibility of the infrastructure.

There is scope yet for many new material compositions through precursor design. Analogous to the influence of precursor design, chemical interactions and modes of decomposition also influence ALD. For example, the rational synthesis of precursors will need to consider control over volatility, decomposition, surface interaction or immobilisation and wetting on the surface of interest. These parameters are especially important in thin film technologies where capacitance, optical transmission, absorption, dielectric constant and defects influence many physical parameters which need to be controlled to a high degree of precision. Polymer-assisted methods offer the possibility of mitigating dewetting phenomena during some methods of coating and subsequent conversion to the active materials from an inorganic precursor, sol or solution. Practically, understanding the evolution and basis of dewetting processes during thermolysis or hydrolysis is important for enhancing uniform surface coverage from dip-coated materials. Recently, several reports have shown that dewetting of thin liquid polymer films could be suppressed by the presence of “inclusions”, which are often nanoparticles.<sup>[117, 192]</sup> Spinodal clustering and nucleation dewetting effects are characterized by specific pattern formation in liquid surface films that eventually solidify. Modern liquid coating investigations address these effects directly, and have demonstrated how pinholes and other defects are minimized in metal oxide thin films formed from liquid precursors due to the formation of nanoscale crystallites of the oxide within the hydrolysing film. This fundamental knowledge is critical for maintaining uniformity within the deposit and as the technologies improve, are paramount for ensuring that crystallinity, doping consistency, phase and composition and other parameters are consistent, especially for very thin films. Dip-coating or spin-casting liquid precursors and nanofluids can in principle be



extended to improve the consistency in sequential or iterative multilayer deposits of hybrid materials and provides a liquid-based route for crystallized thin oxide films with exotic thermal, electrical, and optical properties.

The analytical techniques and recent advances in this review are not limited to solution processed methods only, and serve as a means of directly comparing the depositions to the currently employed techniques, such as sputtering, evaporation and vapour assisted methods. Ultimately, any industrial deposition must involve solution chemistry and the substrate/device geometry. There are challenges that still remain for high speed coating of very large flat panels, and recent research has tackled 3D deposition onto substrates with complex or tortuous geometries. These deposition techniques are becoming increasingly important in photocatalysis, photovoltaics, angle-independent absorber and hole-conducting layers in solar cells, and in water splitting devices. Operational stability of solution processed films in certain electrochemical systems also relies on uniformity in deposition, to avoid pitting, corrosion and localised electric field-induced electrochemistry at grain boundaries, or defects in thin films formed from liquid precursors. Such defects also present reliability and integration challenges for TFT and other electronic devices. New avenues of research that look specifically at methods for stabilization of drying, hydrolysis or polymerizing thin films from liquids are thus of great importance.

For metal oxides, cross-linking between solution chemistry, inorganic syntheses and the (opto)electronic characteristics required by ultra-thin device materials may provide new avenues for non-conventional materials that may be CMOS compatible. Materials systems including mixed metallo-organic precursor systems, alkoxides, carboxylate precursors (long and short chain), and related systems offer advantages during thermolysis similar to ALD precursors, where interaction with the substrate, particularly complex geometrically shaped surfaces, may aid in positioning of the precursors for eventual conversion to the desired oxide

phase. In addition, such phases may be converted to completely transparent films for uniform, well-adhered optical coatings, anti-reflection layers, graded-index sequentially deposited coatings and other applications. Advancements are being made in this regard, using both the film and the substrate co-operatively during crystallization to create a unique completely transparent thin oxide film.

For uniformity in electronic and photonic devices, solubility of all materials in the solvent, i.e., formation of a stable one-pot solution for a range of coating methods requires control of several critical parameters:

- a) The precursor solution must be stable for a long time, for storage and roll-to-roll processing environments for example.
- b) Precursor systems that are 'pure' after thermal treatment/pyrolysis, i.e. only oxygen and the respective metal cation(s) remain to form the uni-, bi-, ternary etc. oxide of choice.
- c) Effects such as macrophase separation, unless wanted, must be avoided or prevented during the drying/thermolysis conversion processes. This may necessitate solution rheology control and the needs to prevent comet defect and streaking during spin coating for example, and solidification at the nozzle of an inkjet printing deposition method where pressure differences corresponds to large temperature changes – the sol or the ink consistency are paramount.
- d) Crack and compositional non-uniformity formation during thermal processing should be prevented, and extension to control of these effects on substrate with flat surfaces and coatings on vertical sidewalls.
- e) Once formed, the films should resist degradation during operation or processing.

In the future, solution processed oxide deposition may facilitate the development of doped metal oxides that use substrate species or indeed the controlled inter-diffusion of species between dissimilar coated layers for diffusional doping, and this may be spatially isolated across a film. Such methods could in principle be extended to polar oxide materials with pyro- and piezoelectric characteristics, high and low-k dielectric materials, nanocrystal embedded dielectrics, and oxide memristors, and the ability to rationally control viscosity to enable or optimize infilling of patterned surfaces or structures for optical coatings, or hard-masks, high density multi TB/sq. inch. materials for magnetic recording etc.

In addition, halted dewetting of multiphasic solution processed materials, may provide embedded materials systems that can approximate composites, providing routes for thermoelectric materials whose phonon scattering and thermal conductivity reduction is based on mesoscale scattering at point defects and compositional variations including grain boundaries caused by phase separation within thin films. Solution processable materials for Li-ion batteries and other composites for energy storage, where mass loading, tap density, thickness and stable connectivity with the substrate are very important, should also be possible with continued research and development.

## **Acknowledgements**

C.G. acknowledges the support of the Irish Research Council under award RS/2011/797. We acknowledge support from the Irish Research Council Ulysses Scheme and from a New Foundations Award. This work was also supported by Science Foundation Ireland (SFI) under the National Access Programme (NAP 417), and through SFI Technology Innovation and Development Awards 2013 and 2015 under contracts 13/TIDA/E2761 and 15/TIDA/2893.

## 7 References

- [1] T. Schneller, R. Waser, M. Kosec, D. Payne, *Chemical Solution Deposition of Functional Oxide Thin Films*, Springer, London **2013**, p. 796.
- [2] E. Fortunato, P. Barquinha, R. Martins, *Adv. Mater.* **2012**, 24, 2945.
- [3] M. S. Bhuiyan, M. Paranthaman, K. Salama, *Supercond. Sci. Technol.* **2006**, 19, R1.
- [4] D. Meyerhofer, *J. Appl. Phys.* **1978**, 49, 3993.
- [5] R. D. Chandra, M. Rao, K. Zhang, R. R. Prabhakar, C. Shi, J. Zhang, S. G. Mhaisalkar, N. Mathews, *ACS Appl. Mater. Interfaces* **2014**, 6, 773.
- [6] K. Si Joon, Y. Seokhyun, K. Hyun Jae, *Jpn. J. Appl. Phys.* **2014**, 53, 02BA02.
- [7] J. S. Park, W.-J. Maeng, H.-S. Kim, J.-S. Park, *Thin Solid Films* **2012**, 520, 1679.
- [8] J. H. Park, J. Y. Oh, S. W. Han, T. I. Lee, H. K. Baik, *ACS Appl. Mater. Interfaces* **2015**, 7, 4494.
- [9] V. Pecunia, K. Banger, H. Siringhaus, *Adv. Electron. Mater.* **2015**, 1, 1400024.
- [10] G. X. Liu, A. Liu, F. K. Shan, Y. Meng, B. C. Shin, E. Fortunato, R. Martins, *Appl. Phys. Lett.* **2014**, 105.
- [11] S. Park, K.-H. Kim, J.-W. Jo, S. Sung, K.-T. Kim, W.-J. Lee, J. Kim, H. J. Kim, G.-R. Yi, Y.-H. Kim, M.-H. Yoon, S. K. Park, *Adv. Func. Mater.* **2015**, 25, 2807.
- [12] C.-P. Chen, Y.-D. Chen, S.-C. Chuang, *Adv. Mater.* **2011**, 23, 3859.
- [13] W. C. H. Choy, D. Zhang, *Small* **2016**, 12, 416.
- [14] M. Faustini, L. Nicole, C. Boissière, P. Innocenzi, C. Sanchez, D. Grosso, *Chem. Mater.* **2010**, 22, 4406.
- [15] C. Glynn, D. Creedon, H. Geaney, E. Armstrong, T. Collins, M. A. Morris, C. O'Dwyer, *Sci. Rep.* **2015**, 5, 11574.
- [16] C. Glynn, D. Creedon, H. Geaney, J. O'Connell, J. D. Holmes, C. O'Dwyer, *ACS Appl. Mater. Interfaces* **2014**, 6, 2031.
- [17] C. J. Brinker, A. J. Hurd, P. R. Schunk, G. C. Frye, C. S. Ashley, *J. Non-Cryst. Solids* **1992**, 147–148, 424.
- [18] P. Nunes, E. Fortunato, R. Martins, *Thin Solid Films* **2001**, 383, 277.
- [19] P. Kregsamer, C. Strelti, P. Wobrauschek, H. Gatterbauer, P. Pianetta, L. Palmetshofer, L. L. Brehm, *X-Ray Spectrom.* **1999**, 28, 292.
- [20] K. H. Zhang, Y. Du, A. Papadogianni, O. Bierwagen, S. Sallis, L. F. Piper, M. E. Bowden, V. Shutthanandan, P. V. Sushko, S. A. Chambers, *Adv. Mater.* **2015**, 27, 5191.
- [21] S. Tepavcevic, H. Xiong, V. R. Stamenkovic, X. Zuo, M. Balasubramanian, V. B. Prakapenka, C. S. Johnson, T. Rajh, *ACS Nano* **2011**, 6, 530.
- [22] C. Glynn, D. Thompson, J. Paez, G. Collins, E. Benavente, V. Lavayen, N. Yutronic, J. D. Holmes, G. Gonzalez, C. O'Dwyer, *J. Mater. Chem. C* **2013**, 1, 5675.
- [23] R. Santos, J. Loureiro, A. Nogueira, E. Elangovan, J. V. Pinto, J. P. Veiga, T. Busani, E. Fortunato, R. Martins, I. Ferreira, *Appl. Surf. Sci.* **2013**, 282, 590.
- [24] S. R. Thomas, P. Pattanasattayavong, T. D. Anthopoulos, *Chem. Soc. Rev.* **2013**, 42, 6910.
- [25] P. K. Nayak, J. A. Caraveo-Frescas, Z. Wang, M. N. Hedhili, Q. X. Wang, H. N. Alshareef, *Sci. Rep.* **2014**, 4, 4672.
- [26] E. M. C. Fortunato, P. M. C. Barquinha, A. C. M. B. G. Pimentel, A. M. F. Gonçalves, A. J. S. Marques, L. M. N. Pereira, R. F. P. Martins, *Adv. Mater.* **2005**, 17, 590.
- [27] C. M. Eliason, M. D. Shawkey, *Opt. Express* **2014**, 22, A642.
- [28] H. Song, L. Guo, Z. Liu, K. Liu, X. Zeng, D. Ji, N. Zhang, H. Hu, S. Jiang, Q. Gan, *Adv. Mater.* **2014**, 26, 2737.
- [29] J. Q. Xi, M. F. Schubert, J. K. Kim, E. F. Schubert, M. Chen, S.-Y. Lin, LiuW, J. A. Smart, *Nat. Photon.* **2007**, 1, 176.

- [30] V. Shrotriya, G. Li, Y. Yao, C. W. Chu, Y. Yang, *Appl. Phys. Lett.* **2006**, 88, 073508.
- [31] J. Meyer, S. Hamwi, M. Kröger, W. Kowalsky, T. Riedl, A. Kahn, *Adv. Mater.* **2012**, 24, 5408.
- [32] C. H. Choi, S. Y. Han, Y. W. Su, Z. Fang, L. Y. Lin, C. C. Cheng, C. H. Chang, *J. Mater. Chem. C* **2015**, 3, 854.
- [33] F. Jiang, W. C. H. Choy, X. Li, D. Zhang, J. Cheng, *Adv. Mater.* **2015**, 27, 2930.
- [34] F. Xie, W. C. H. Choy, C. Wang, X. Li, S. Zhang, J. Hou, *Adv. Mater.* **2013**, 25, 2051.
- [35] C. G. Granqvist, *Thin Solid Films* **2014**, 564, 1.
- [36] F. F. Abdi, L. Han, A. H. M. Smets, M. Zeman, B. Dam, R. van de Krol, *Nat. Commun.* **2013**, 4, 2195.
- [37] S. Hu, M. R. Shaner, J. A. Beardslee, M. Lichterman, B. S. Brunshwig, N. S. Lewis, *Science* **2014**, 344, 1005.
- [38] G. H. Jeon, *J. Phys. D: Appl. Phys.* **2009**, 42, 043001.
- [39] T. D. Manning, I. P. Parkin, R. J. H. Clark, D. Sheel, M. E. Pemble, D. Vernadou, *J. Mater. Chem. A* **2002**, 12, 2936.
- [40] R. W. Johnson, A. Hultqvist, S. F. Bent, *Mater. Today* **2014**, 17, 236.
- [41] C. Ba, S. T. Bah, M. D'Auteuil, P. V. Ashrit, R. Vallee, *ACS Appl. Mater. Interfaces* **2013**, 5, 12520.
- [42] E. M. C. Fortunato, P. M. C. Barquinha, A. C. M. B. G. Pimentel, A. M. F. Gonçalves, A. J. S. Marques, R. F. P. Martins, L. M. N. Pereira, *Appl. Phys. Lett.* **2004**, 85, 2541.
- [43] M. Leskelä, M. Ritala, *Thin Solid Films* **2002**, 409, 138.
- [44] N. Deepak, M. A. Caro, L. Keeney, M. E. Pemble, R. W. Whatmore, *Adv. Func. Mater.* **2014**, 24, 2844.
- [45] Y. Wei, M. Li, J. Zheng, C. Xu, *Thin Solid Films* **2013**, 534, 446.
- [46] W. Xu, H. Wang, F. Xie, J. Chen, H. Cao, J.-B. Xu, *ACS Appl. Mater. Interfaces* **2015**, 7, 5803.
- [47] H. Faber, Y.-H. Lin, S. R. Thomas, K. Zhao, N. Pliatsikas, M. A. McLachlan, A. Amassian, P. A. Patsalas, T. D. Anthopoulos, *ACS Appl. Mater. Interfaces* **2015**, 7, 782.
- [48] C. Glynn, D. Aureau, S. O'Hanlon, L. Daly, H. Geaney, G. Collins, A. Etcheberry, C. O'Dwyer, *ECS Trans.* **2015**, 64, 1.
- [49] F. F. Lange, *Science* **1996**, 273, 903.
- [50] J. Livage, C. Sanchez, *J. Non-Cryst. Solids* **1992**, 145, 11.
- [51] M. Nabavi, S. Doeuff, C. Sanchez, J. Livage, *J. Non-Cryst. Solids* **1990**, 121, 31.
- [52] C. Sanchez, J. Livage, M. Henry, F. Babonneau, *J. Non-Cryst. Solids* **1988**, 100, 65.
- [53] J.-W. Jo, J. Kim, K.-T. Kim, J.-G. Kang, M.-G. Kim, K.-H. Kim, H. Ko, Y.-H. Kim, S. K. Park, *Adv. Mater.* **2015**, 27, 1182.
- [54] M.-G. Kim, M. G. Kanatzidis, A. Facchetti, T. J. Marks, *Nat. Mater.* **2011**, 10, 382.
- [55] Q. X. Jia, T. M. McCleskey, A. K. Burrell, Y. Lin, G. E. Collis, H. Wang, A. D. Q. Li, S. R. Foltyn, *Nat. Mater.* **2004**, 3, 529.
- [56] A. K. Burrell, T. Mark McCleskey, Q. X. Jia, *Chem. Comm.* **2008**, 1271.
- [57] S. O'Hanlon, C. Glynn, C. O'Dwyer, *ECS J. Solid State Sci. Technol.* **2015**, 5, R3100.
- [58] M. Alsawafta, A. Almoabadi, S. Badilescu, V.-V. Truong, *J. Electrochem. Soc* **2015**, 162, H466.
- [59] T. J. Hanlon, R. E. Walker, J. A. Coath, M. A. Richardson, *Thin Solid Films* **2002**, 405, 234.
- [60] C.-C. Chueh, C.-Z. Li, A. K. Y. Jen, *Energy Environ. Sci.* **2015**, 8, 1160.
- [61] Y. Si, Z. Guo, *Nanoscale* **2015**, 7, 5922.
- [62] L. Hu, H. Wu, F. La Mantia, Y. Yang, Y. Cui, *ACS Nano* **2010**, 4, 5843.

- [63] S. Bae, H. Kim, Y. Lee, X. Xu, J.-S. Park, Y. Zheng, J. Balakrishnan, T. Lei, H. Ri Kim, Y. I. Song, Y.-J. Kim, K. S. Kim, B. Ozyilmaz, J.-H. Ahn, B. H. Hong, S. Iijima, *Nat. Nano.* **2010**, 5, 574.
- [64] F. C. Krebs, J. Fyenbo, M. Jorgensen, *J. Mater. Chem.* **2010**, 20, 8994.
- [65] F. C. Krebs, *Sol. Energy Mater. Sol. Cells* **2009**, 93, 394.
- [66] N. A. Chang, J. J. Richardson, P. G. Clem, J. W. P. Hsu, *Small* **2006**, 2, 75.
- [67] D. Zhang, W. C. H. Choy, F.-x. Xie, X. Li, *Org. Electron.* **2012**, 13, 2042.
- [68] R. E. Schaak, T. E. Mallouk, *Chem. Mater.* **2000**, 12, 2513.
- [69] C. Pacholski, A. Kornowski, H. Weller, *Angew. Chem. Int. Ed.* **2002**, 41, 1188.
- [70] D. Birnie, III, S. Hau, D. Kamber, D. Kaz, *J. Mater. Sci. Mater.* **2005**, 16, 715.
- [71] A. G. Emslie, F. T. Bonner, L. G. Peck, *J. Appl. Phys.* **1958**, 29, 858.
- [72] C. J. Brinker, G. C. Frye, A. J. Hurd, C. S. Ashley, *Thin Solid Films* **1991**, 201, 97.
- [73] L. Landau, B. Levich, *Acta Physicochim. URSS* **1942**, 17, 12.
- [74] M. Faustini, B. Louis, P. A. Albouy, M. Kuemmel, D. Grosso, *J. Phys. Chem. C* **2010**, 114, 7637.
- [75] F. Nishida, B. Dunn, J. M. McKiernan, J. I. Zink, C. J. Brinker, A. J. Hurd, *J. Sol-Gel Sci. Technol.* **1994**, 2, 477.
- [76] J. H. Alan, in *The Colloid Chemistry of Silica*, Vol. 234, American Chemical Society, 1994, 433.
- [77] A. J. Hurd, C. J. Brinker, *J. Phys. France* **1988**, 49, 1017.
- [78] M. Faustini, D. R. Ceratti, B. Louis, M. Boudot, P.-A. Albouy, C. Boissière, D. Grosso, *ACS Appl. Mater. Interfaces* **2014**, 6, 17102.
- [79] F. Ye, C. Cui, A. Kirkemide, D. Dong, M. M. Collinson, D. A. Higgins, *Chem. Mater.* **2010**, 22, 2970.
- [80] D. R. Ceratti, B. Louis, X. Paquez, M. Faustini, D. Grosso, *Adv. Mater.* **2015**, 27, 4958.
- [81] N. J. Arfsten, A. Eberle, J. Otto, A. Reich, *J. Sol-Gel Sci. Technol.* **1997**, 8, 1099.
- [82] Y. Wang, T. J. McCarthy, *Langmuir* **2014**, 30, 2419.
- [83] D. Perednis, L. Gauckler, *J. Electroceram.* **2005**, 14, 103.
- [84] C. H. Chen, E. M. Kelder, J. Schoonman, *J. Mater. Sci. Lett.* **1997**, 16, 1967.
- [85] S. P. S. Arya, H. E. Hintermann, *Thin Solid Films* **1990**, 193–194, Part 2, 841.
- [86] B. Wang, X. Yu, P. Guo, W. Huang, L. Zeng, N. Zhou, L. Chi, M. J. Bedzyk, R. P. H. Chang, T. J. Marks, A. Facchetti, *Adv. Electron. Mater.* **2016**, 2.
- [87] X. Liu, T.-J. Tarn, F. Huang, J. Fan, *Particuology* **2015**, 19, 1.
- [88] B.-J. de Gans, U. S. Schubert, *Macromol. Rapid Commun.* **2003**, 24, 659.
- [89] C.-H. Choi, L.-Y. Lin, C.-C. Cheng, C.-h. Chang, *ECS J. Solid State Sci. Technol.* **2015**, 4, P3044.
- [90] H. W. Choi, T. Zhou, M. Singh, G. E. Jabbour, *Nanoscale* **2015**, 7, 3338.
- [91] P. Calvert, *Chem. Mater.* **2001**, 13, 3299.
- [92] D. H. Lee, Y. J. Chang, G. S. Herman, C. H. Chang, *Adv. Mater.* **2007**, 19, 843.
- [93] A. T. Findikoglu, Q. X. Jia, D. W. Reagor, X. D. Wu, *Microw. Opt. Techn. Lett.* **1995**, 9, 306.
- [94] P. Zhai, Q. Yi, J. Jian, H. Wang, P. Song, C. Dong, X. Lu, Y. Sun, J. Zhao, X. Dai, Y. Lou, H. Yang, G. Zou, *Chem. Comm.* **2014**, 50, 1854.
- [95] S. Beke, *Thin Solid Films* **2011**, 519, 1761.
- [96] D. McNulty, D. N. Buckley, C. O'Dwyer, *J. Power Sources* **2014**, 267, 831.
- [97] M. Armstrong, C. O'Dwyer, W. Macklin, J. D. Holmes, *Nano Res.* **2014**, 7, 1.
- [98] C. O'Dwyer, V. Lavayen, D. A. Tanner, S. B. Newcomb, E. Benavente, G. González, C. M. S. Torres, *Adv. Func. Mater.* **2009**, 19, 1736.

- [99] M. B. Sahana, C. Sudakar, C. Thapa, G. Lawes, V. M. Naik, R. J. Baird, G. W. Auner, R. Naik, K. R. Padmanabhan, *Mater. Sci. Eng., B* **2007**, 143, 42.
- [100] A. G. Souza Filho, O. P. Ferreira, E. J. G. Santos, J. Mendes Filho, O. L. Alves, *Nano Lett.* **2004**, 4, 2099.
- [101] J. Huotari, J. Lappalainen, J. Puustinen, A. Lloyd Spetz, *Sens. Actuators, B* **2013**, 187, 386.
- [102] V. Lavayen, C. O'Dwyer, G. Cárdenas, G. González, C. M. Sotomayor Torres, *Mater. Res. Bull.* **2007**, 42, 674.
- [103] C. O'Dwyer, V. Lavayen, S. B. Newcomb, M. A. Santa Ana, E. Benavente, G. González, C. M. Sotomayor Torres, *J. Electrochem. Soc.* **2007**, 154, K29.
- [104] A. A. Akl, *Appl. Surf. Sci.* **2006**, 252, 8745.
- [105] R. Irani, S. M. Rozati, S. Beke, *Mater. Chem. Phys.* **2013**, 139, 489.
- [106] Y. D. Ji, T. S. Pan, Z. Bi, W. Z. Liang, Y. Zhang, H. Z. Zeng, Q. Y. Wen, H. W. Zhang, C. L. Chen, Q. X. Jia, Y. Lin, *Appl. Phys. Lett.* **2012**, 101, 071902.
- [107] J. Livage, *Chem. Mater.* **1991**, 3, 578.
- [108] J. Livage, *Coord. Chem. Rev.* **1999**, 190–192, 391.
- [109] S.-P. Cho, J.-S. Yeo, D.-Y. Kim, S.-i. Na, S.-S. Kim, *Sol. Energy Mater. Sol. Cells* **2015**, 132, 196.
- [110] K. Zilberberg, S. Trost, J. Meyer, A. Kahn, A. Behrendt, D. Lützenkirchen-Hecht, R. Frahm, T. Riedl, *Adv. Func. Mater.* **2011**, 21, 4776.
- [111] C. Costa, C. Pinheiro, I. Henriques, C. A. T. Laia, *ACS Appl. Mater. Interfaces* **2012**, 4, 5266.
- [112] J. Livage, *Materials* **2010**, 3, 4175.
- [113] C. K. Chan, H. Peng, R. D. Twesten, K. Jarausch, X. F. Zhang, Y. Cui, *Nano Lett.* **2007**, 7, 490.
- [114] K. Chebout, A. Iratni, A. Bouremana, S. Sam, A. Keffous, N. Gabouze, *Solid State Ionics* **2013**, 253, 164.
- [115] F. P. Gökdemir, O. Özdemir, K. Kutlu, *Electrochim. Acta* **2014**, 121, 240.
- [116] K. Zilberberg, S. Trost, H. Schmidt, T. Riedl, *Adv. Energy Mater.* **2011**, 1, 377.
- [117] G. Amarandei, C. O'Dwyer, A. Arshak, U. Thiele, U. Steiner, D. Corcoran, *Langmuir* **2013**, 29, 6706.
- [118] A. Bouzidi, N. Benramdane, A. Nakrela, C. Mathieu, B. Khelifa, R. Desfeux, A. Da Costa, *Mater. Sci. Eng., B* **2002**, 95, 141.
- [119] A. Chidembo, S. H. Aboutalebi, K. Konstantinov, M. Salari, B. Winton, S. A. Yamini, I. P. Nevirkovets, H. K. Liu, *Energy Environ. Sci.* **2012**, 5, 5236.
- [120] H. S. Lim, D. Kwak, D. Y. Lee, S. G. Lee, K. Cho, *J. Am. Chem. Soc.* **2007**, 129, 4128.
- [121] J. Tauc, *The Optical Properties of Solids*, Academic Press, New York **1966**, p.
- [122] T. S. Moss, *Phys. Status Solidi B* **1985**, 131, 415.
- [123] N. M. Ravindra, P. Ganapathy, J. Choi, *Infrared Phys. Techn.* **2007**, 50, 21.
- [124] R. R. Reddy, Y. Nazeer Ahammed, *Infrared Phys. Techn.* **1995**, 36, 825.
- [125] C. Glynn, D. Aureau, G. Collins, S. O'Hanlon, A. Etcheberry, C. O'Dwyer, *Nanoscale* **2015**, 7, 20227.
- [126] Z. Zhan, J. Cao, W. Xie, L. Hou, Q. Ye, P. Liu, *J. Nanomater.* **2014**, 2014, 1.
- [127] C. V. Ramana, R. J. Smith, O. M. Hussain, C. C. Chusuei, C. M. Julien, *Chem. Mater.* **2005**, 17, 1213.
- [128] I. Hancox, L. A. Rochford, D. Clare, M. Walker, J. J. Mudd, P. Sullivan, S. Schumann, C. F. McConville, T. S. Jones, *J. Phys. Chem. C* **2013**, 117, 49.
- [129] X. Bao, Q. Zhu, T. Wang, J. Guo, C. Yang, D. Yu, N. Wang, W. Chen, R. Yang, *ACS Appl. Mater. Interfaces* **2015**, 7, 7613.

- [130] Y. Kuo, *Electrochem. Soc. Interface* **2013**, 22, 55.
- [131] Y. Kuo, *Thin film transistors. 1. Amorphous silicon thin film transistors*, Vol. 1, Springer Science & Business Media, **2004**, p.
- [132] Y. Kuo, P. M. Kozlowski, *Appl. Phys. Lett.* **1996**, 69, 1092.
- [133] W. Xu, H. Wang, L. Ye, J. Xu, *J. Mater. Chem. C* **2014**, 2, 5389.
- [134] K. K. Banger, Y. Yamashita, K. Mori, R. L. Peterson, T. Leedham, J. Rickard, H. Siringhaus, *Nat. Mater.* **2011**, 10, 45.
- [135] W.-J. Lee, W.-T. Park, S. Park, S. Sung, Y.-Y. Noh, M.-H. Yoon, *Adv. Mater.* **2015**, 27, 5043.
- [136] J. Yu, G. Liu, A. Liu, Y. Meng, B. Shin, F. Shan, *J. Mater. Chem. C* **2015**.
- [137] J. Li, S. Q. Wang, J. W. Mayer, K. N. Tu, *Phys. Rev. B* **1989**, 39, 12367.
- [138] Y. H. Kim, J. S. Heo, T. H. Kim, S. Park, M. H. Yoon, J. Kim, M. S. Oh, G. R. Yi, Y. Y. Noh, S. K. Park, *Nature* **2012**, 489, 128.
- [139] T. Clark, J. D. Ruiz, H. Fan, C. J. Brinker, B. I. Swanson, A. N. Parikh, *Chem. Mater.* **2000**, 12, 3879.
- [140] N. Mizoshita, M. Ishii, N. Kato, H. Tanaka, *ACS Appl. Mater. Interfaces* **2015**, 7, 19424.
- [141] E. Fortunato, A. Gonçalves, A. Pimentel, P. Barquinha, G. Gonçalves, L. Pereira, I. Ferreira, R. Martins, *Appl. Phys. A* **2009**, 96, 197.
- [142] X. Yu, L. Zeng, N. Zhou, P. Guo, F. Shi, D. B. Buchholz, Q. Ma, J. Yu, V. P. Dravid, R. P. Chang, M. Bedzyk, T. J. Marks, A. Facchetti, *Adv. Mater.* **2015**, 27, 2390.
- [143] J. Jang, R. Kitsomboonloha, S. L. Swisher, E. S. Park, H. Kang, V. Subramanian, *Adv. Mater.* **2013**, 25, 1042.
- [144] D. R. Lide, *CRC handbook of chemistry and physics*, CRC press, **2004**, p.
- [145] N. N. Greenwood, A. Earnshaw, *Chemistry of the Elements*, Elsevier, **2012**, p.
- [146] R. M. Pasquarelli, D. S. Ginley, R. O'Hayre, *Chem. Soc. Rev.* **2011**, 40, 5406.
- [147] Z. Chen, W. Li, R. Li, Y. Zhang, G. Xu, H. Cheng, *Langmuir* **2013**, 29, 13836.
- [148] C. O'Dwyer, C. Sotomayor Torres, *Front. Phys.* **2013**, 1, 1
- [149] T. O. L. Sunde, E. Garskaite, B. Otter, H. E. Fossheim, R. Saeterli, R. Holmestad, M.-A. Einarsrud, T. Grande, *J. Mater. Chem.* **2012**, 22, 15740.
- [150] S. Watcharotone, D. A. Dikin, S. Stankovich, R. Piner, I. Jung, G. H. B. Dommett, G. Evmenenko, S.-E. Wu, S.-F. Chen, C.-P. Liu, S. T. Nguyen, R. S. Ruoff, *Nano Lett.* **2007**, 7, 1888.
- [151] A. Kim, Y. Won, K. Woo, C.-H. Kim, J. Moon, *ACS Nano* **2013**, 7, 1081.
- [152] C. O'Dwyer, M. Szachowicz, G. Visimberga, V. Lavayen, S. B. Newcomb, C. M. S. Torres, *Nat. Nano.* **2009**, 4, 239.
- [153] K. Ellmer, *Nat. Photon* **2012**, 6, 809.
- [154] J. H. Chang, K. M. Chiang, H. W. Kang, W. J. Chi, J. H. Chang, C. I. Wu, H. W. Lin, *Nanoscale* **2015**, 7, 4572.
- [155] C. G. Granqvist, *Handbook of inorganic electrochromic materials*, Elsevier, **1995**, p.
- [156] Z. Tong, J. Hao, K. Zhang, J. Zhao, B.-L. Su, Y. Li, *J. Mater. Chem. C* **2014**, 2, 3651.
- [157] Y. Wang, K. Takahashi, K. H. Lee, G. Z. Cao, *Adv. Func. Mater.* **2006**, 16, 1133.
- [158] C. Costa, C. Pinheiro, I. Henriques, C. A. T. Laia, *ACS Appl. Mater. Interfaces* **2012**, 4, 1330.
- [159] E. L. Miller, *Energ. Environ. Sci.* **2015**, 8, 2809.
- [160] Y. Wang, L. Liu, L. Xu, X. Cao, X. Li, Y. Huang, C. Meng, Z. Wang, W. Zhu, *Nanoscale* **2014**, 6, 6790.
- [161] S. G. Kumar, L. G. Devi, *J. Phys. Chem. A* **2011**, 115, 13211.
- [162] Q. Peng, B. Kalanyan, P. G. Hoertz, A. Miller, D. H. Kim, K. Hanson, L. Alibabaei, J. Liu, T. J. Meyer, G. N. Parsons, J. T. Glass, *Nano Lett.* **2013**, 13, 1481.



- [163] M. Arin, P. Lommens, N. Avci, S. C. Hopkins, K. De Buysser, I. M. Arabatzis, I. Fasaki, D. Poelman, I. Van Driessche, *J. Eur. Ceram. Soc.* **2011**, 31, 1067.
- [164] T. Ameri, G. Dennler, C. Lungenschmied, C. J. Brabec, *Energy Environ. Sci.* **2009**, 2, 347.
- [165] J. H. Kim, P. W. Liang, S. T. Williams, N. Cho, C. C. Chueh, M. S. Glaz, D. S. Ginger, A. K. Jen, *Adv. Mater.* **2015**, 27, 695.
- [166] X. C. Li, F. X. Xie, S. Q. Zhang, J. H. Hou, W. C. H. Choy, *Light-Sci. Appl.* **2015**, 4, 273.
- [167] W. Chen, Y. Wu, Y. Yue, J. Liu, W. Zhang, X. Yang, H. Chen, E. Bi, I. Ashraful, M. Grätzel, L. Han, *Science* **2015**, 350, 944.
- [168] J. You, L. Meng, T.-B. Song, T.-F. Guo, Y. Yang, W.-H. Chang, Z. Hong, H. Chen, H. Zhou, Q. Chen, Y. Liu, N. De Marco, Y. Yang, *Nat. Nano.* **2016**, 11, 75.
- [169] H.-L. Yip, A. K. Y. Jen, *Energ. Environ. Sci.* **2012**, 5, 5994.
- [170] L. Lu, T. Xu, I. H. Jung, L. Yu, *J. Phys. Chem. C* **2014**, 118, 22834.
- [171] S. Y. Liu, S. H. Ho, Y. Chen, F. So, *Chem. Mater.* **2015**, 27, 2532.
- [172] Q. Yi, P. Zhai, Y. Sun, Y. Lou, J. Zhao, B. Sun, B. Patterson, H. Luo, W. Zhang, L. Jiao, H. Wang, G. Zou, *ACS Appl. Mater. Interfaces* **2015**, 7, 18218.
- [173] L. Trotochaud, J. K. Ranney, K. N. Williams, S. W. Boettcher, *J. Am. Chem. Soc.* **2012**, 134, 17253.
- [174] M. Abbasi, S. M. Rozati, R. Irani, S. Beke, *Mater. Sci. Semicond. Process.* **2015**, 29, 132.
- [175] E. Armstrong, C. O'Dwyer, *J. Mater. Chem. C* **2015**, 3, 6109.
- [176] E. Armstrong, M. Osiak, H. Geaney, C. Glynn, C. O'Dwyer, *CrystEngComm* **2014**, 16, 10804.
- [177] F. Niklaus, C. Vieider, H. Jakobsen, *Proc. SPIE 6836* **2007**, 6836, 68360.
- [178] M. Sung, H. Kwang, L. Minbaek, C. Yun-Hyuk, H. Seong-Hyeon, H. Seunghun, *Nanotechnology* **2007**, 18, 205304.
- [179] N. Vieira, W. Avansi, A. Figueiredo, C. Ribeiro, V. Mastelaro, F. Guimarães, *Nanoscale Res. Lett.* **2012**, 7, 1.
- [180] A. O. Cetinkaya, S. Kaya, A. Aktag, E. Budak, E. Yilmaz, *Thin Solid Films* **2015**, 590, 7.
- [181] G. Gu, M. Schmid, P. W. Chiu, A. Minett, J. Fraysse, G. T. Kim, S. Roth, M. Kozlov, E. Munoz, R. H. Baughman, *Nat. Mater* **2003**, 2, 316.
- [182] J. Livage, *Nat. Mater.* **2003**, 2, 297.
- [183] R. H. Baughman, C. Cui, A. A. Zakhidov, Z. Iqbal, J. N. Barisci, G. M. Spinks, G. G. Wallace, A. Mazzoldi, D. De Rossi, A. G. Rinzler, O. Jaschinski, S. Roth, M. Kertesz, *Science* **1999**, 284, 1340.
- [184] R. H. Baughman, *Science* **2005**, 308, 63.
- [185] M. D. Bhatt, C. O'Dwyer, *Phys. Chem. Chem. Phys.* **2015**, 17, 4799.
- [186] M. Osiak, H. Geaney, E. Armstrong, C. O'Dwyer, *J. Mater. Chem. A* **2014**, 2, 9433.
- [187] W. McSweeney, O. Lotty, C. Glynn, H. Geaney, J. D. Holmes, C. O'Dwyer, *Electrochim. Acta* **2014**, 135, 356.
- [188] W. McSweeney, H. Geaney, C. O'Dwyer, *Nano Res.* **2015**, 8, 1395.
- [189] A. M. Gaikwad, A. C. Arias, D. A. Steingart, *Energy Technol.* **2015**, 3, 305.
- [190] K. Brezesinski, J. Haetge, J. Wang, S. Mascotto, C. Reitz, A. Rein, S. H. Tolbert, J. Perlich, B. Dunn, T. Brezesinski, *Small* **2011**, 7, 407.
- [191] J. Leppaniemi, O. H. Huttunen, H. Majumdar, A. Alastalo, *Adv. Mater.* **2015**, 27, 7168.
- [192] G. Amarandei, C. O'Dwyer, A. Arshak, D. Corcoran, *ACS Appl. Mater. Interfaces* **2013**, 5, 8655.

## Figure captions

**Figure 1.** The different steps involved for the deposition of thin films through solution processed techniques. Each of the steps is outlined in the different sections of this review.

**Figure 2.** Examples of different applications exploiting a thin film materials intercalative, electronic and optical properties through different device architectures.

**Figure 3.** Schematic of the basic steps in preparing a solution processable precursor solution.

**Figure 4.** (a) Schematic of process steps involved in the formation of thin films through spin coating. (b) Graphs showing how thin film thickness is influenced by both spin speed and duration, adapted from ref. 3.<sup>[3]</sup> (c) How fluid of ethanol thickness evolves with respect to time at constant acceleration to 2000 RPM, from ref. 70.<sup>[70]</sup> The cross-over point signifies when the dominating process controlling film thickness changes from liquid flow to evaporation.

**Figure 5.** (a) Schematic of thin film formation from a dip-coating technique. The solid thin film forms through evaporation and condensation of the solvent from a dip-coated liquid film. (b) Schematic for steady state dip-coating processes showing the forces which control the thin film formation (ref 17).<sup>[17]</sup> (c) Plot of thickness versus withdrawal speed, with modelled fits, for a variety of liquid precursor systems showing the characteristic trend for dip-coated thin film formation, adapted from ref. 74.<sup>[74]</sup> (d) Schematic of the processes controlling thin film formation in fast- and slow-rate deposition regimes, adapted from ref. 15.<sup>[15]</sup>

**Figure 6.** Optical images and schematic outlining the formation mechanism of a thin film from an alkoxide based precursor solution. Reproduced with permission from ref. 15.<sup>[15]</sup>







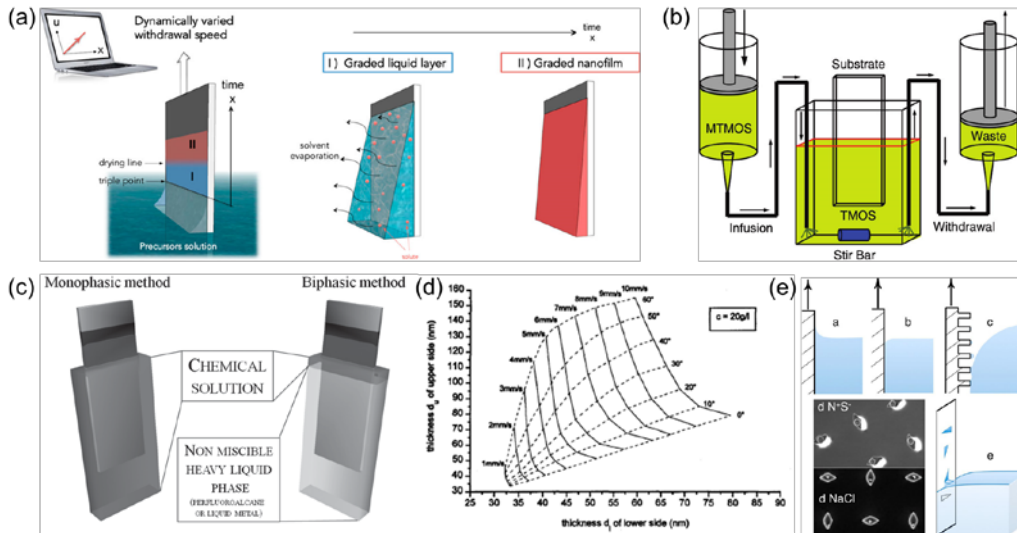


Figure 7. Various innovative techniques for altering dip-coated thin films. (a) Preparing graded thin films through varying withdrawal speed in-situ. Reproduced with permission from ref. 78.<sup>[78]</sup> (b) Infusion withdrawal technique where a secondary material is infused into the solution during dip-coating. Reproduced with permission from ref. 79.<sup>[79]</sup> (c) Large surface thin film coating technique using minimal precursor solution through use of a biphasic solution. Reproduced with permission from ref. 80.<sup>[80]</sup> (d) Influence on both upper and lower surface thin films on the angle during angle-dependent dip-coating. Reproduced with permission from ref. 81.<sup>[81]</sup> (e) Schematic of the deposition of chemically treated surfaces where a mix of hydrophobic and hydrophilic surfaces are dip-coated. Reproduced with permission from ref. 82.<sup>[82]</sup>

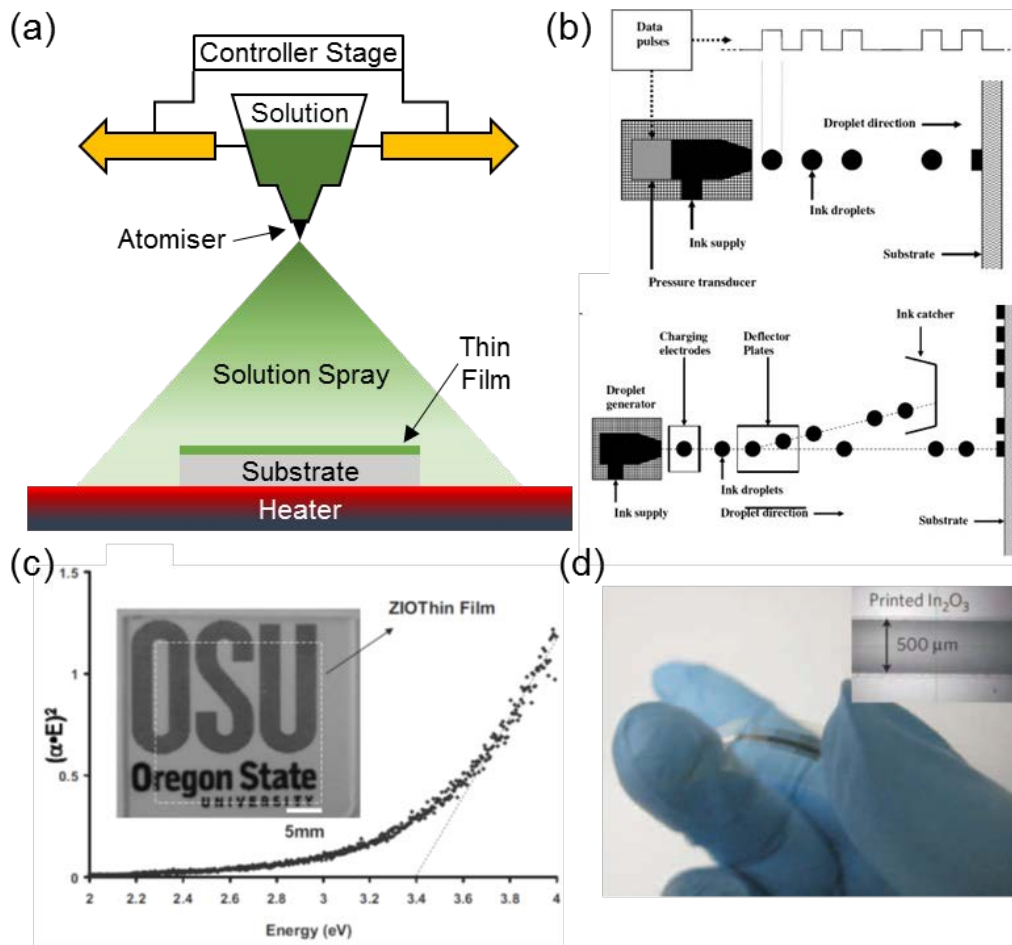


Figure 8. Schematic representations of (a) spray pyrolysis and (b) two ink-jet printing, both on-demand (top) and continuous (bottom), thin film deposition techniques. Reproduced with permission from ref. 65.<sup>[65]</sup> (c) Optical bandgap measurement and optical image for a inkjet printed ZIO thin film. Reproduced with permission from ref. 92.<sup>[92]</sup> (d) Optical image of a flexible In<sub>2</sub>O<sub>3</sub> TFT with the inset showing an ink-jet printed In<sub>2</sub>O<sub>3</sub> line. Reproduced with permission from ref. 54.<sup>[54]</sup>

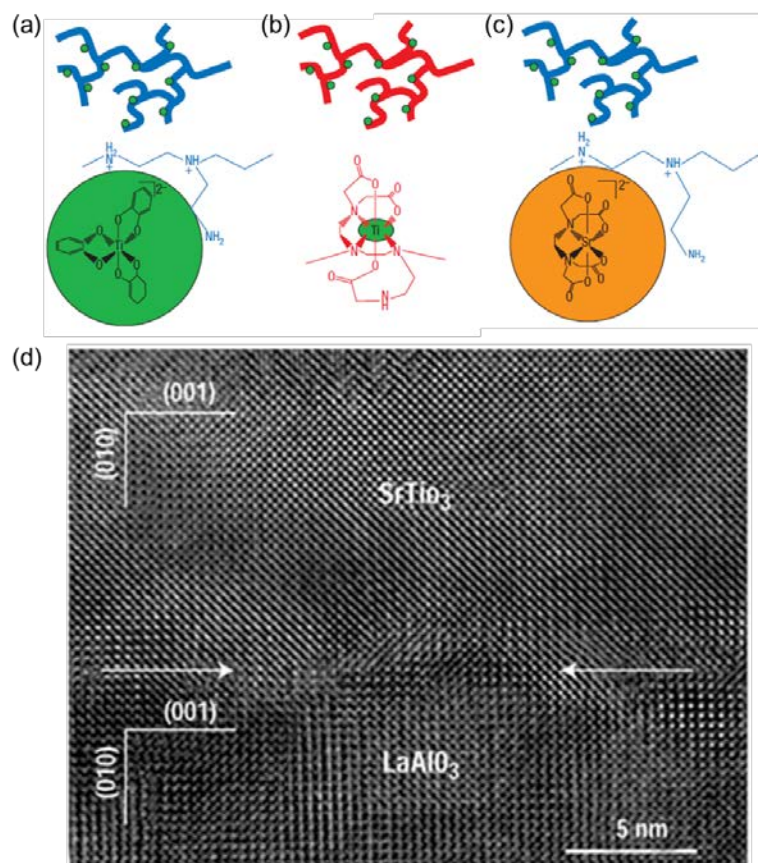


Figure 9. Schematic of PAD process for Ti metal ions. (a) Ti bound to PEI as a catecholate ion and to (b) PEIC directly. (c) Strontium, as an EDTA complex, bound to PEI. (d) HRTEM image of epitaxial deposition using PAD processes of SrTiO<sub>3</sub> on LaAlO<sub>3</sub>. Reproduced with permission from ref. 55.<sup>[55]</sup>



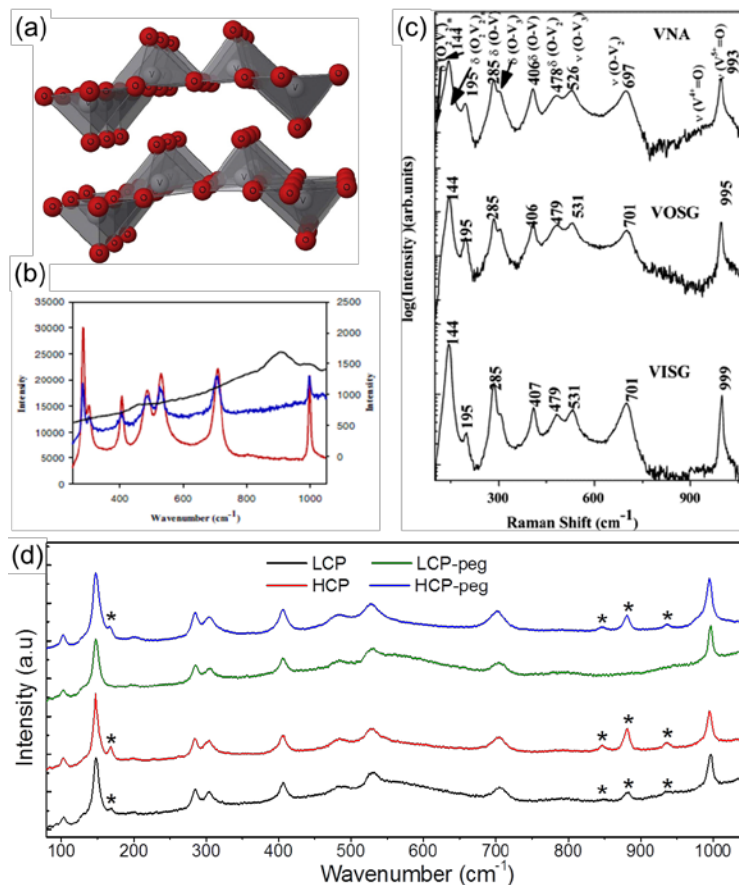


Figure 10. (a) Structural schematic of two layers of  $V_2O_5$  with V atoms (grey) and O atoms (red). Reproduced with permission from ref. 95.<sup>[95]</sup> (b) Raman scattering spectra of dip-coated  $V_2O_5$  thin films as-deposited (black) and annealed at both 300 °C (blue) and 500 °C (red). Reproduced with permission from ref. 58.<sup>[58]</sup> (c) Raman scattering spectra of spin coated  $V_2O_5$  thin films formed from a metallo-organic (VNA), organic (VOSG) and inorganic (VISG) based precursor solution. Reproduced with permission from ref. 99.<sup>[99]</sup> (d) Raman scattering spectra of dip-coated  $V_2O_5$  thin films deposited at low concentration (LCP) and high concentration (HCP) ratios with/without PEG addition. Extra vibrations present in the spectra attributed to vanadyl-oxygen bond displacement are highlighted with an asterisk (\*). Reproduced with permission from ref. 15.<sup>[15]</sup>

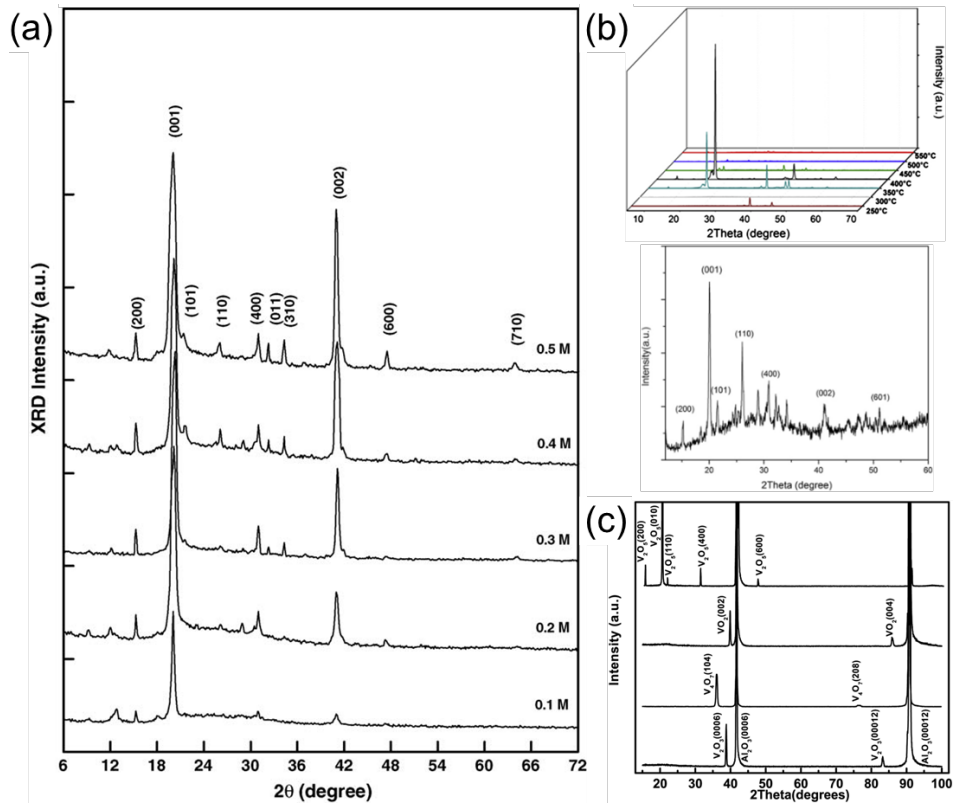


Figure 11. XRD pattern of  $V_2O_5$  thin films showing effects of varying the (a) precursor solution concentration, (b) substrate temperature and (c) substrate and processing condition to form multiple VO materials. Reproduced with permission from refs 104, 105 and 106 respectively.<sup>[104-106]</sup> (a, b) were deposited using a spray pyrolysis technique and (c) was deposited through a spin coating/PAD technique.

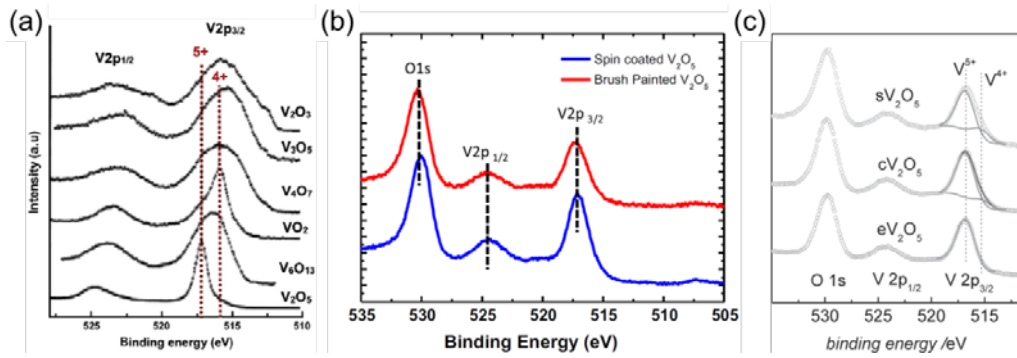


Figure 12. XPS spectra of the O 1s and V 2p for VO thin films. (a) XPS spectra of  $V_2O_5$  compared to a variety of other vanadium oxide structures. Reproduced with permission from ref. 95.<sup>[95]</sup> (b) Comparison between two solution processed techniques; spin coated and brush painted  $V_2O_5$  thin films. Reproduced with permission from ref. 109.<sup>[109]</sup> (c) Comparison between evaporation deposited ( $eV_2O_5$ ,  $vV_2O_5$ ) and spin coated ( $sV_2O_5$ ) thin films. Reproduced with permission from ref. 110.<sup>[110]</sup>

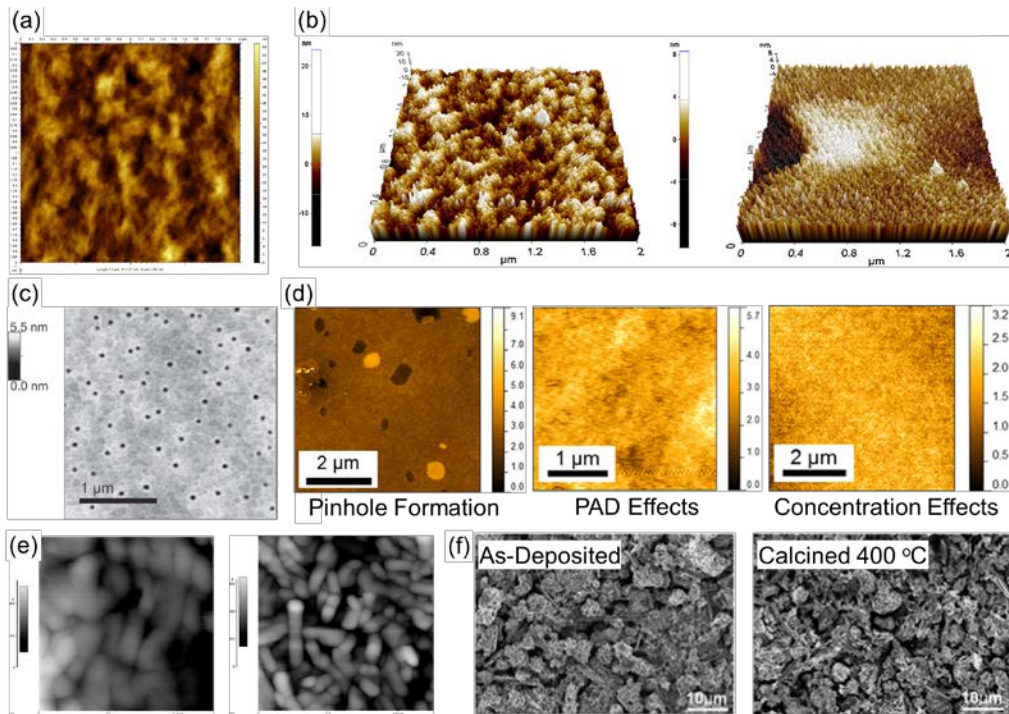


Figure 13. AFM and SEM Images highlighting the possible  $V_2O_5$  surface morphologies formed using a variety of solution processed deposition techniques, namely (a) ink-jet printing (b) dip-coating of two different precursor solutions, (c) spin-coating, (d) dip-coating showing PAD and precursor concentration effects, (e) spray pyrolysis of two different molar concentrations and (f) drop casted  $V_2O_5$  precursor solution. Reproduced with permission from refs 111, 115, 116, 16, 118 and 120 respectively.<sup>[16, 111, 115-116, 118, 120]</sup>

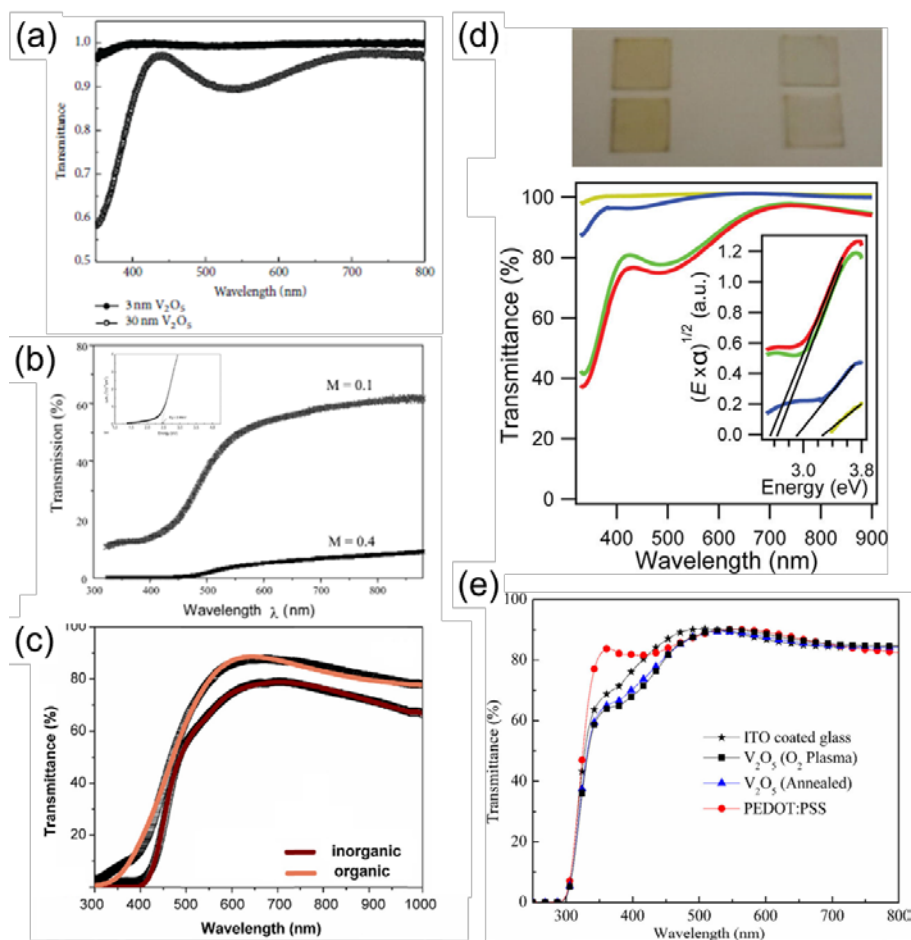


Figure 14. UV-Vis transmission spectra and associated analysis for a variety of  $V_2O_5$  thin films deposited using a variety of techniques with some comparisons to contemporary materials and non-solution processable methods. (a) Transmission comparison of a 3 nm and 30 nm thick  $V_2O_5$  sputtered thin film showing the changes in optical transmission characteristics. Reproduced with permission from ref 126.<sup>[126]</sup> (b) Changes in transmission due to concentration changes using spray pyrolysis and associated Tauc plot for  $V_2O_5$  (inset). Reproduced with permission from ref 118.<sup>[118]</sup> (c) Transmission for dip-coated  $V_2O_5$  thin films formed from inorganic and organic based precursors. Reproduced with permission from ref 115.<sup>[115]</sup> (d) Optical images and corresponding transmission and Tauc analysis for a variety of  $V_2O_5$  thin films spin coated and annealed under varied atmospheric conditions. Reproduced with permission from ref 128.<sup>[128]</sup> (e) Transmission images for spin coated  $V_2O_5$  thin film treated under different post-processing conditions thin films compared to both ITO coated glass and PEDOT:PSS. Reproduced with permission from ref 129.<sup>[129]</sup>

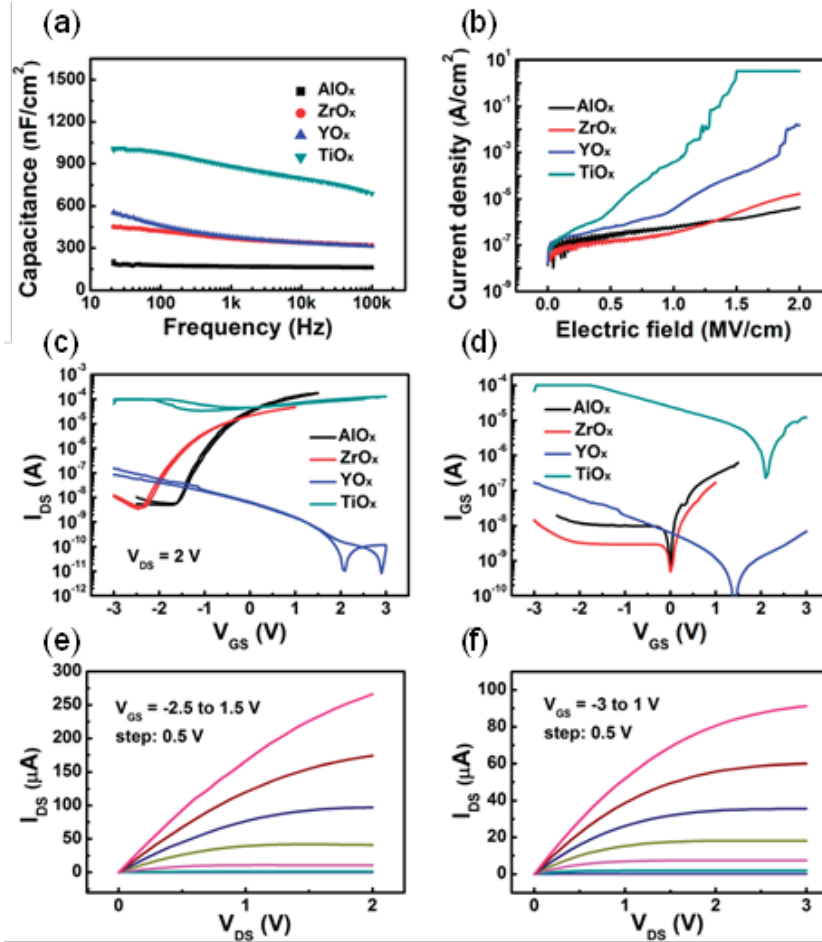


Figure 15. Electrical characteristics of different solution processed high-k dielectric materials showing the (a) capacitance vs. frequency, (b) leakage current density vs. electric field. (c) Transfer characteristics and (d) gate leakage characteristics of In<sub>2</sub>O<sub>3</sub> TFTs with high-k solution processed dielectrics. Output characteristics of In<sub>2</sub>O<sub>3</sub> TFTs with (e) AlO<sub>x</sub> and (f) ZrO<sub>x</sub> dielectrics. Reproduced with permission from ref 133.<sup>[133]</sup>

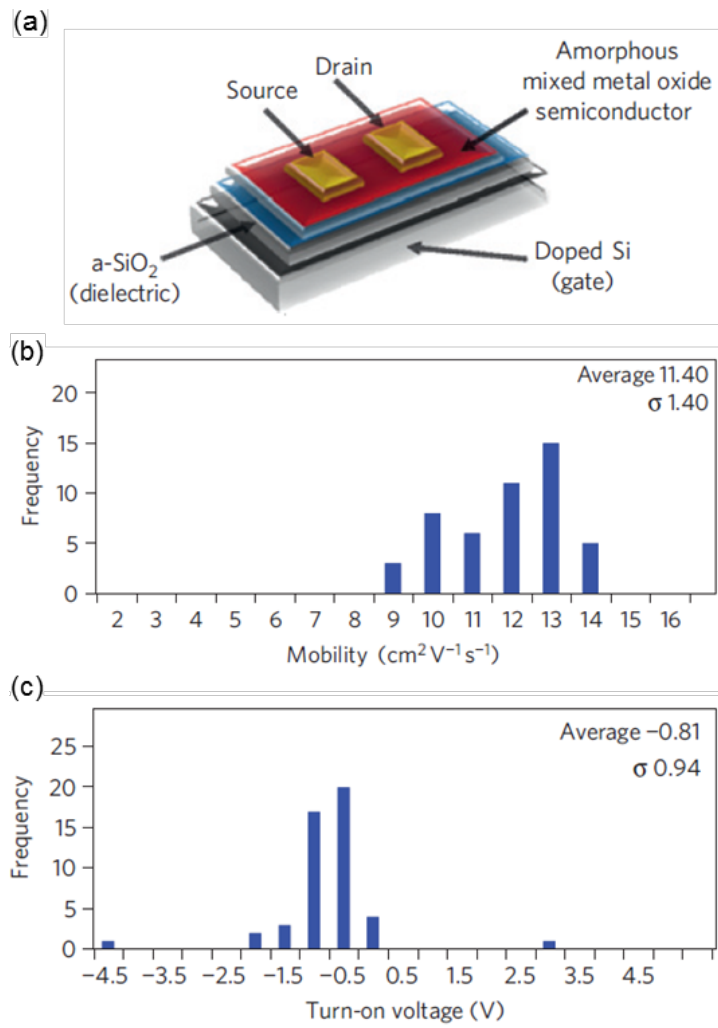


Figure 16. (a) IZO TFT device architecture and histograms of 49 IZO TFTs displaying their (b) mobility and (c) turn on voltages. Reproduced with permission from ref 134.<sup>[134]</sup>

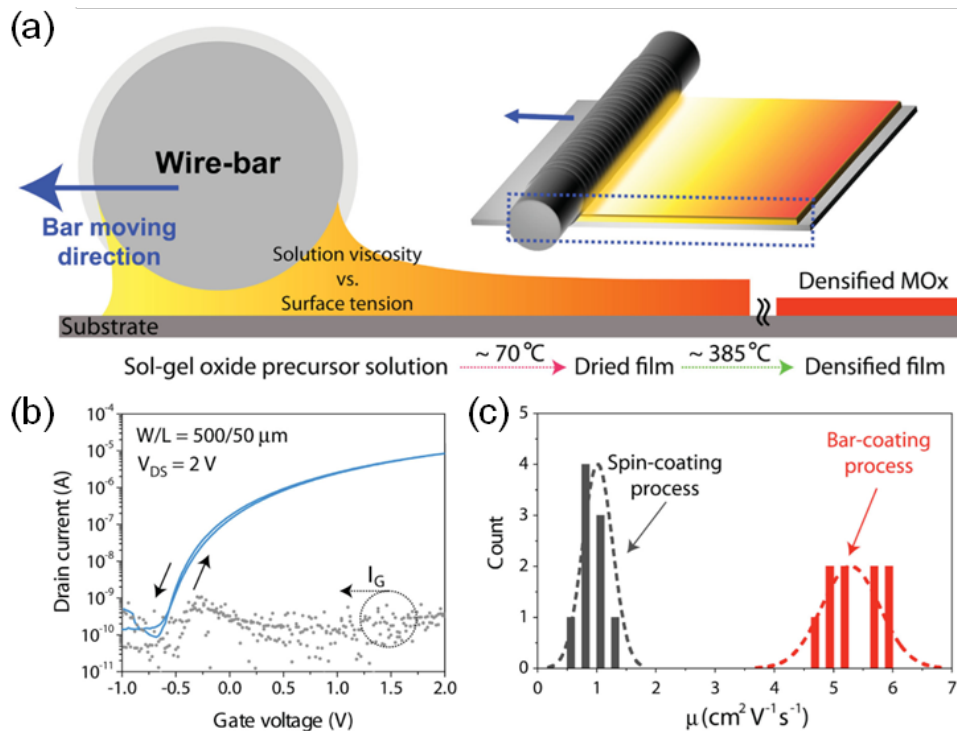


Figure 17. (a) Schematic for preparing thin films using a bar-coater system. (b) Representative transfer and output characteristics for all-bar-coated metal oxide TFTs. (c) Comparison of statistical distributions for TFT mobility values for IGZO TFTs using either spin-coating or bar-coating deposition techniques. Reproduced with permission from ref 135.<sup>[135]</sup>



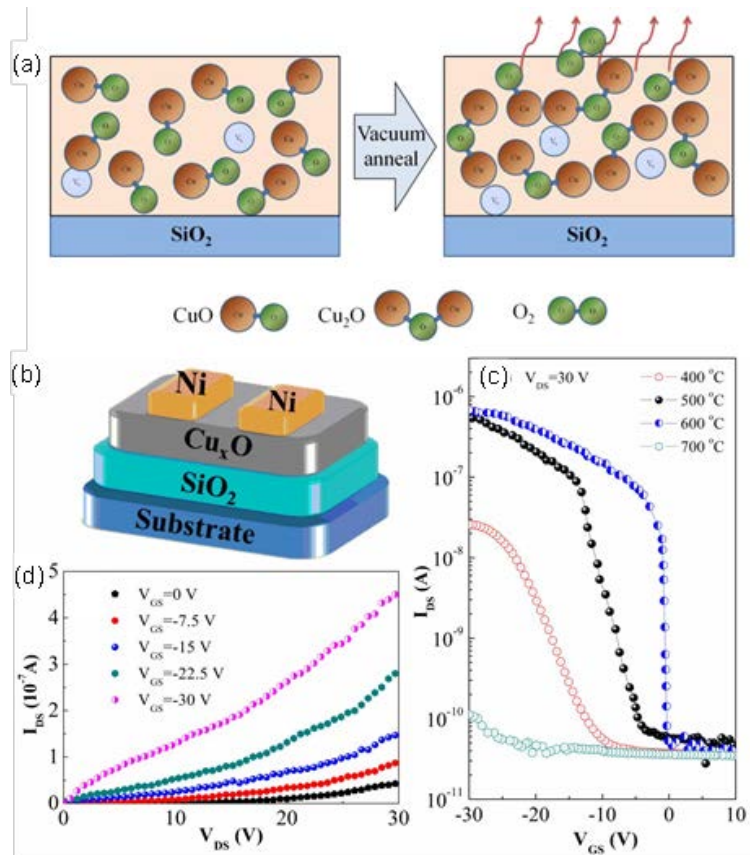


Figure 18. Schematic of Cu<sub>x</sub>O thin films showing (a) effect of vacuum-annealing on thin film structure and (b) Cu<sub>x</sub>O TFT diagram. (c) Transfer characteristics of Cu<sub>x</sub>O thin films prepared at various thin film annealing temperatures under vacuum and (d) output characteristics of the same TFT annealed at 600 °C. Reproduced with permission from ref 136.<sup>[136]</sup>

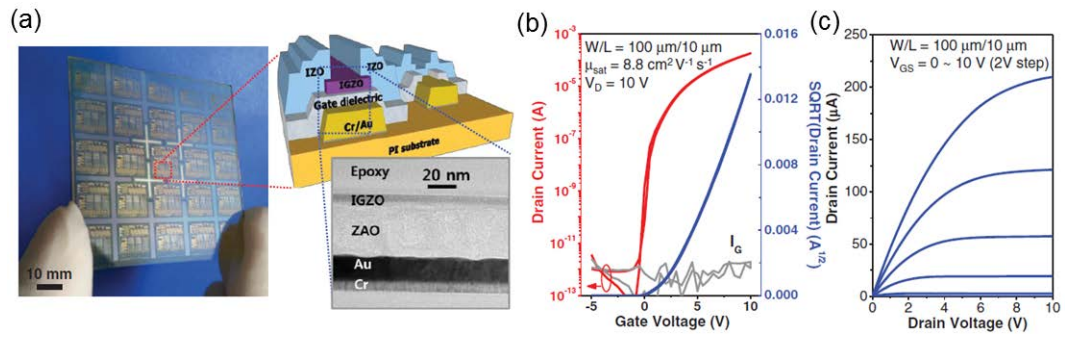


Figure 19. Spin coated IGZO TFTs and circuits on PI substrate. (a) Optical image, schematic and corresponding TEM cross-section. (b) Transfer and (c) output characteristics of IGZO TFTs with ZAO dielectric layer. Reproduced with permission from ref 53.<sup>[53]</sup>

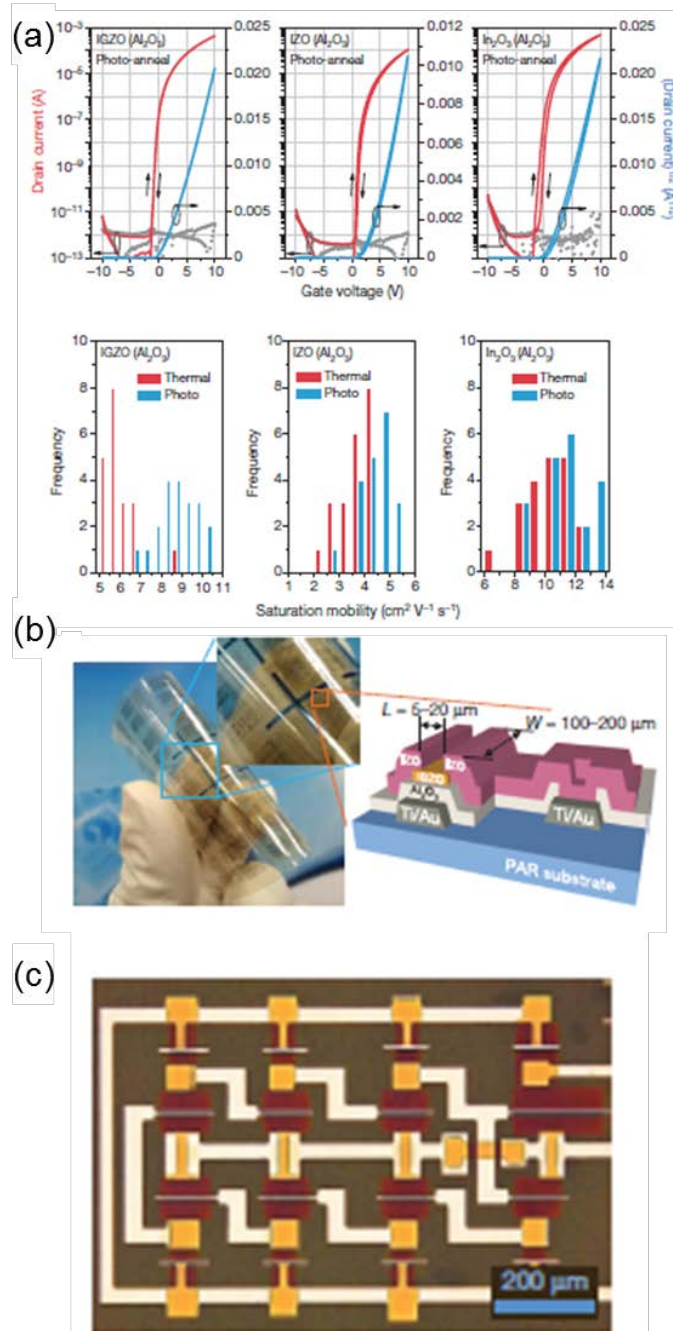


Figure 20. (a) Transfer characteristics and distribution of saturation mobility for both photo- and thermal-annealed GZO, IZO and In<sub>2</sub>O<sub>3</sub> TFTs with an Al<sub>2</sub>O<sub>3</sub> gate dielectric. (b) Optical image and schematic of IGZO TFTs and circuits on a flexible PAR polymer substrate and (c) zoomed in optical image of one of the seven-stage ring oscillator. Reproduced with permission from ref 138.<sup>[138]</sup>

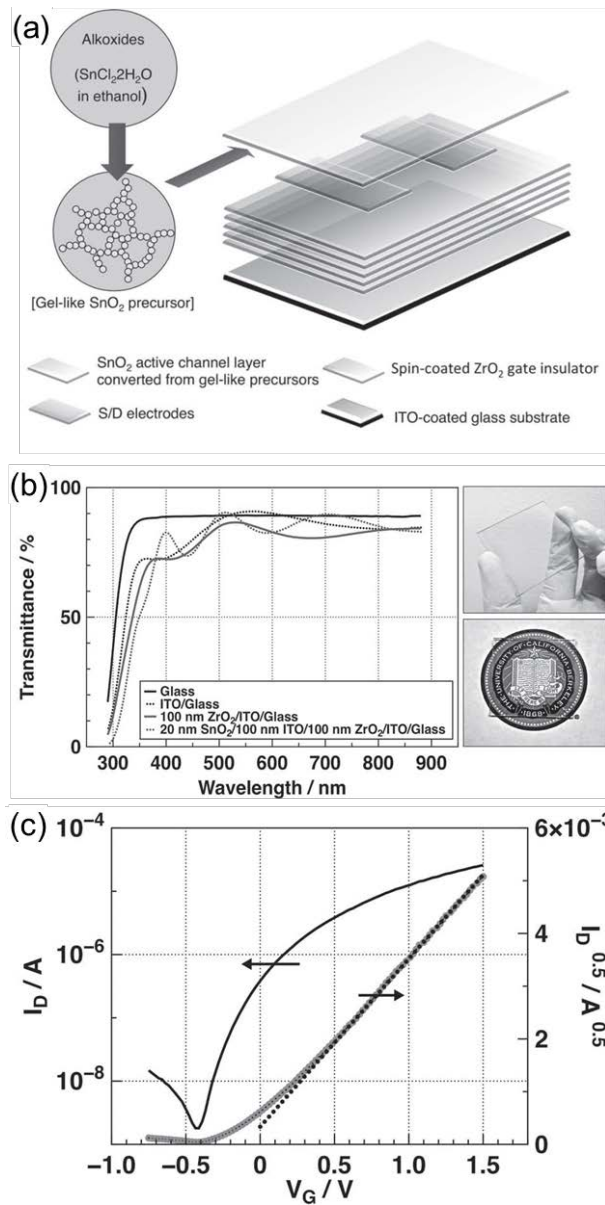


Figure 21. (a) Fully Transparent SnO<sub>2</sub>/ZrO<sub>2</sub> TFT schematic and (b) accompanying optical transmission spectroscopy and images of the TFTs with ITO source and drain electrodes. (c) Transfer characteristics of SnO<sub>2</sub>/ZrO<sub>2</sub> TFT devices. Reproduced with permission from ref 143.<sup>[143]</sup>

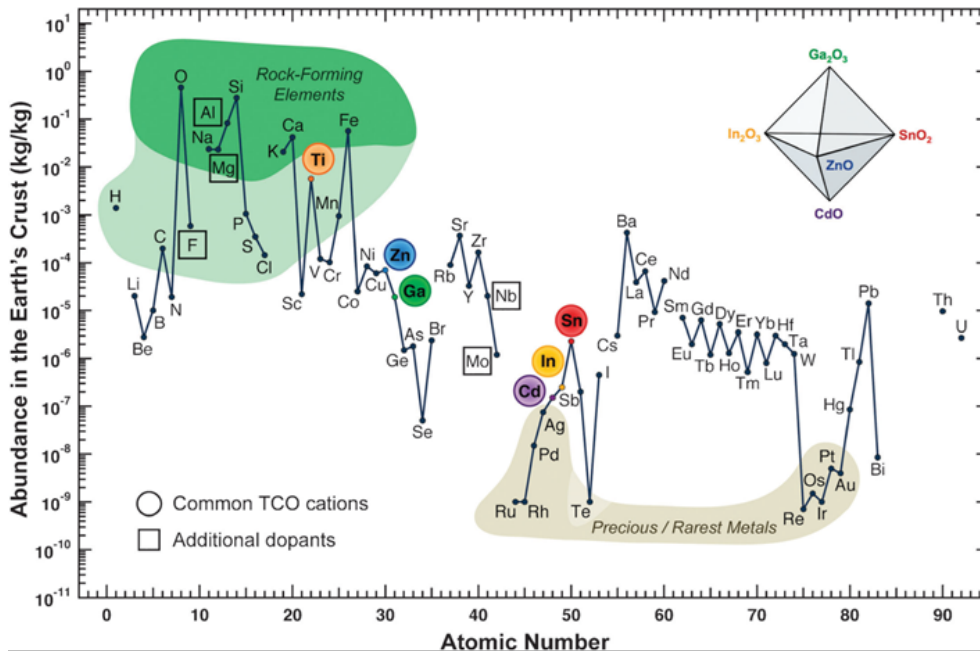


Figure 22. Mass fraction abundance of elements in the Earth's crust in relation to their atomic number. The common TCO cations are highlighted by coloured circles with additional possible dopants shown with squares. Adapted and reproduced with permission from refs 144, 145 and 146.<sup>[144-146]</sup>

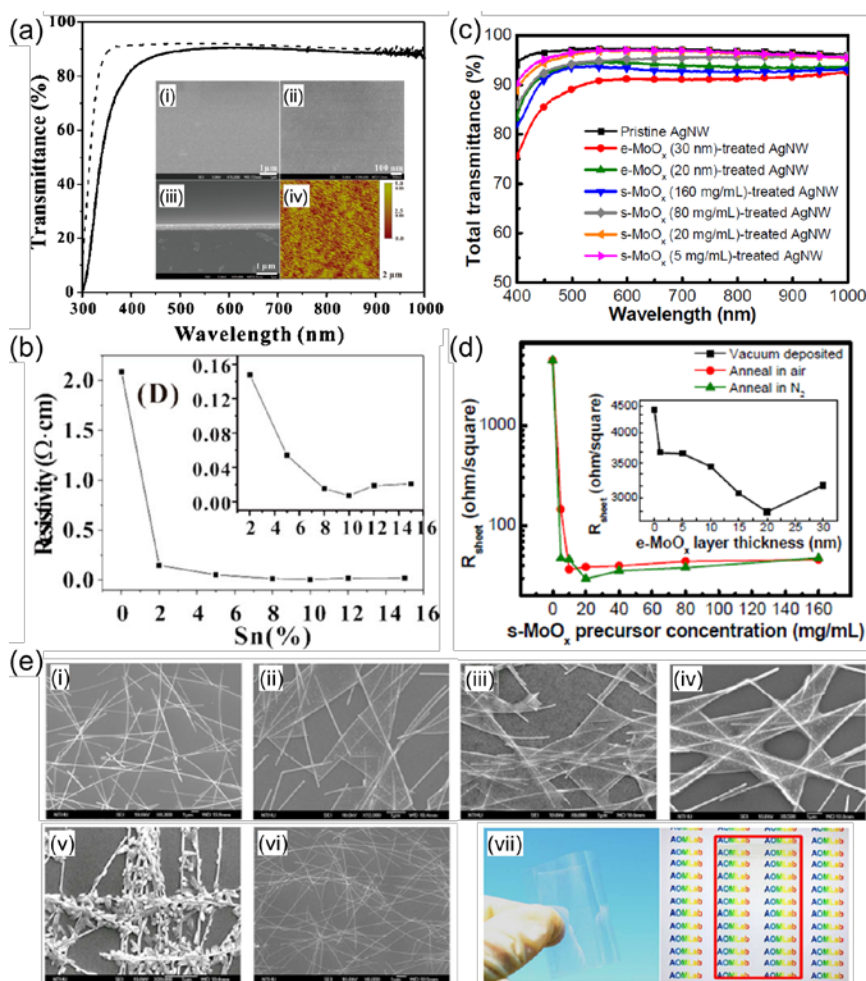


Figure 23. (a) ITO thin film UV-Vis transparency and SEM images of a Sn% = 10% with the accompanying glass spectra included. (b) The effect of increased Sn% on the resistivity of the ITO thin film. (a-b) reproduced with permission from ref 147.<sup>[147]</sup> (c) UV-Vis transparency of pristine AgNW and  $\text{MoO}_x$  treated AgNWs and (d) thin film resistivity vs.  $\text{MoO}_x$  precursor concentration. (e) SEM images of (i) pristine AgNWs and AgNWs coated with  $\text{MoO}_x$  at concentrations of (ii) 5 mg/ml, (iii) 20 mg/ml, (iv) 40 mg/ml, (v) 160 mg/ml and (vi) evaporated 30 nm thin film. (vii) Optical images of flexible TCO material composed of AgNWs coated with  $\text{MoO}_x$  on a PEN substrate. (c-e) reproduced with permission from ref 154.<sup>[154]</sup>





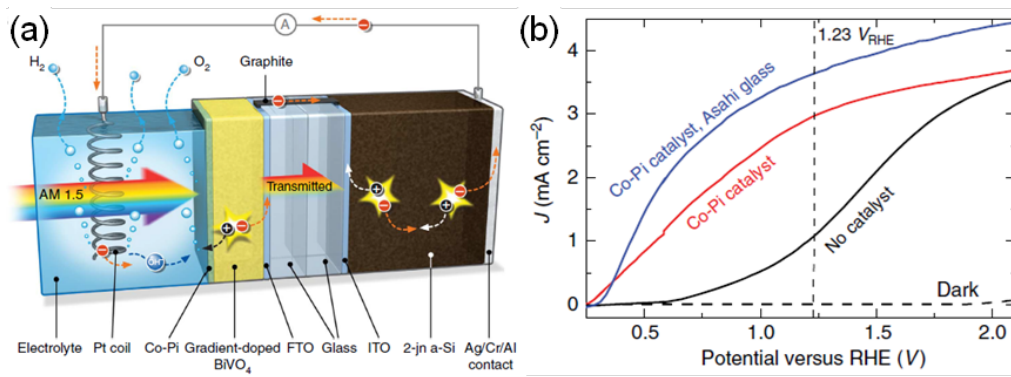


Figure 25. (a) A schematic representation of a combined gradient-doped W:BiVO<sub>4</sub> and amorphous-Si solar cell. (b) Photocurrent vs. voltage curve of un-catalysed and Co-Pi-catalysed gradient doped W:BiVO<sub>4</sub> electrodes. The black and red lines are for devices deposited on TEC-15 with the blue line data deposited on conductive glass substrates. Reproduced with permission from ref 36.<sup>[36]</sup>



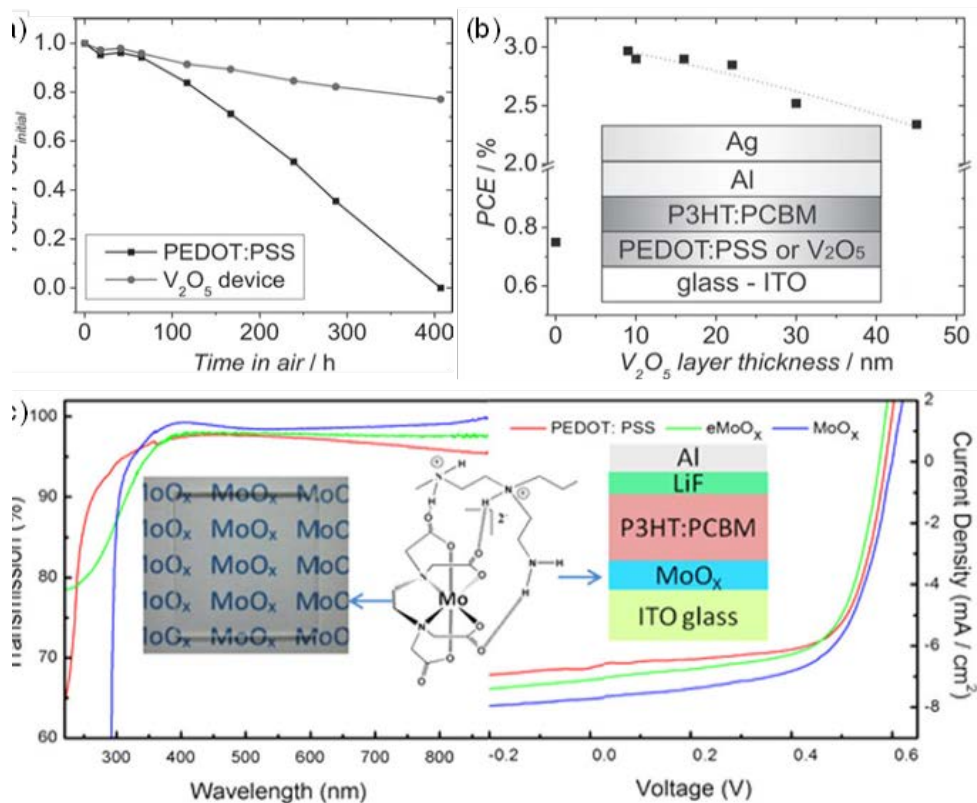


Figure 26. (a) Power conversion efficiency of organic solar cells utilising either a PEDOT:PSS or V<sub>2</sub>O<sub>5</sub> hole extraction layer in an ambient air atmosphere. (b) Power conversion efficiency of the same organic solar cells with increasing thickness of V<sub>2</sub>O<sub>5</sub> hole extraction layer. Also included is the efficiency with no V<sub>2</sub>O<sub>5</sub> layer. (a-b) reproduced with permission from ref 116.<sup>[116]</sup> (c) UV-Vis Transmission of PEDOT:PSS, evaporated and spin-coated/PAD MoO<sub>x</sub> (included optical image) thin films. Characteristic current density vs. voltage for the three types of films used as interfacial layers in organic solar cells. Reproduced with permission from ref 172.<sup>[172]</sup>

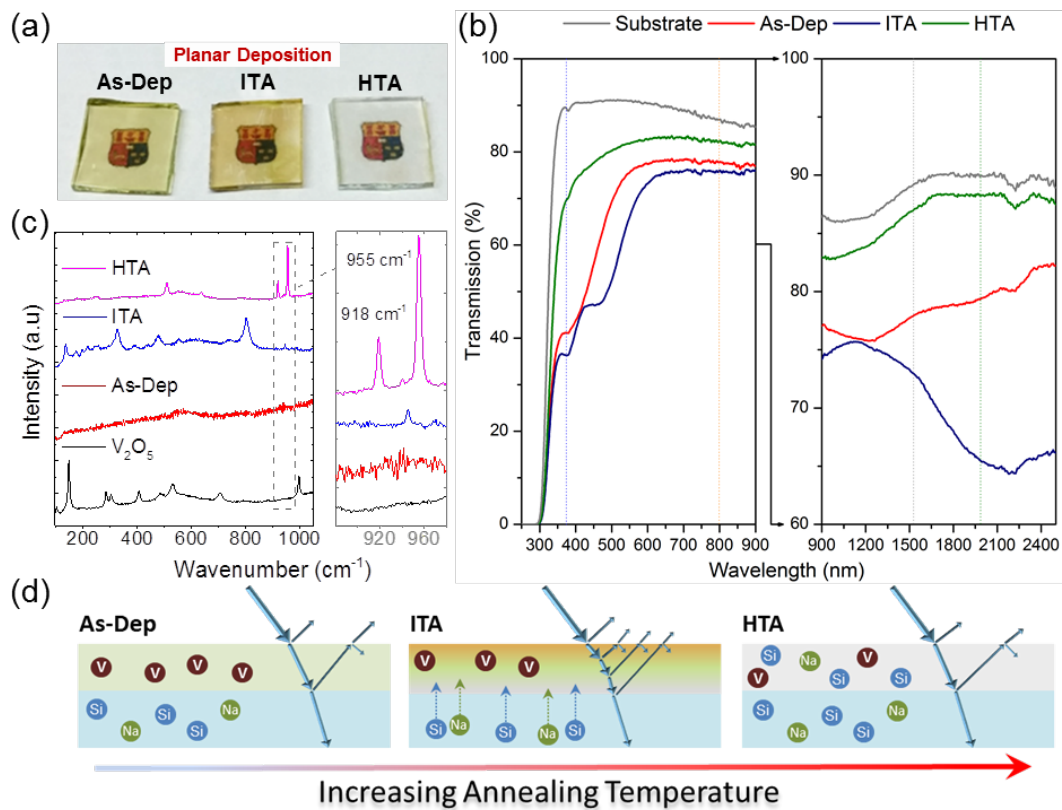


Figure 27. (a) Optical images of the formation of a transparent thin film through an inter-diffusion process at an intermediate (ITA) and high (HTA) thermal annealing temperature. (b) UV-Vis-NIR of the inter-diffused thin film compared to the glass substrate. (c) Raman scattering spectroscopy of the inter-diffused thin film showing the formation of NaVO<sub>3</sub> within a glassy matrix. (d) Schematic detailing the formation of the transparent thin film through inter-diffusion processes. Reproduced with permission from ref 125.<sup>[125]</sup>

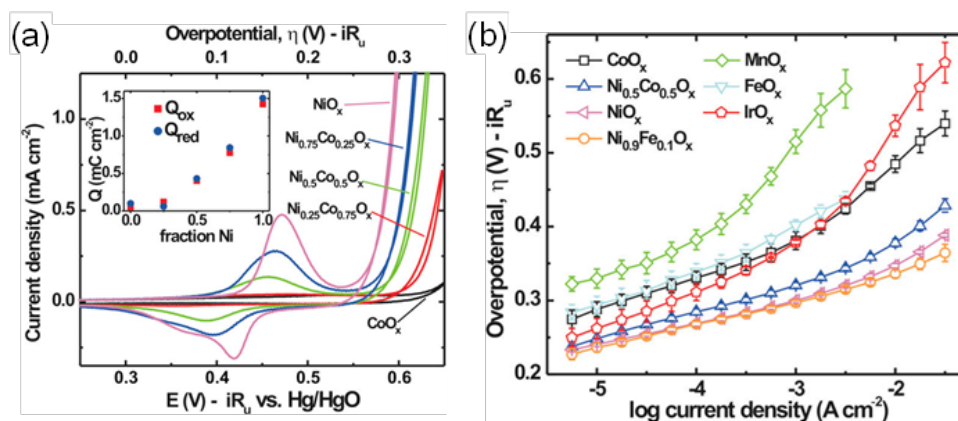


Figure 28. (a) Voltammetry of a number of conditioned thin films with differing Ni contents for electrocatalytic testing with an integrated charge for the redox processes as a function of Ni content. (b) Comparison of steady state Tafel measurements for different thin films in 1 M KOH. Reproduced with permission from ref 173.<sup>[173]</sup>

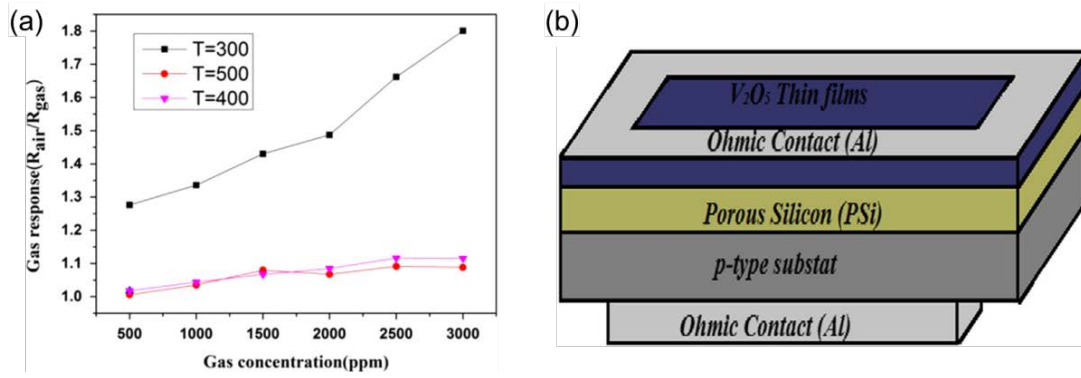


Figure 29. (a) Sensing response curve as a function of ethanol concentration for  $V_2O_5$  based thin film sensors deposited through spray pyrolysis at different pyrolysis temperatures. Reproduced with permission from ref 174.<sup>[174]</sup> (b) Schematic of a proposed  $V_2O_5$ /porous Si/Si ethanol sensor. Reproduced with permission from ref 114.<sup>[114]</sup>

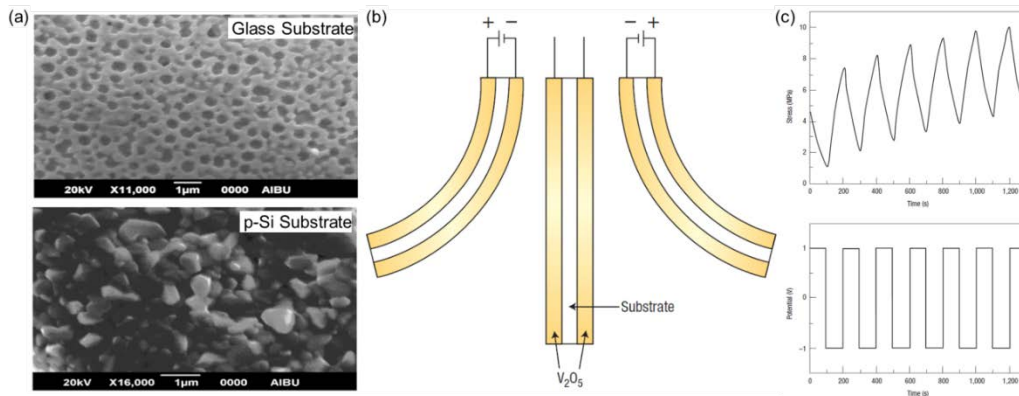


Figure 30. (a) SEM images of solution processed  $\text{BiFeO}_3$  thin films deposited on glass and p-Si substrates for use as capacitor electrodes. Reproduced with permission from ref 180.<sup>[180]</sup> (b) Schematic of a  $\text{V}_2\text{O}_5$  free standing cantilever actuator and (c) Generated stress (top) and corresponding applied potential (bottom) as a function of time. (b-c) Reproduced with permission from refs 181 and 182.<sup>[181-182]</sup>

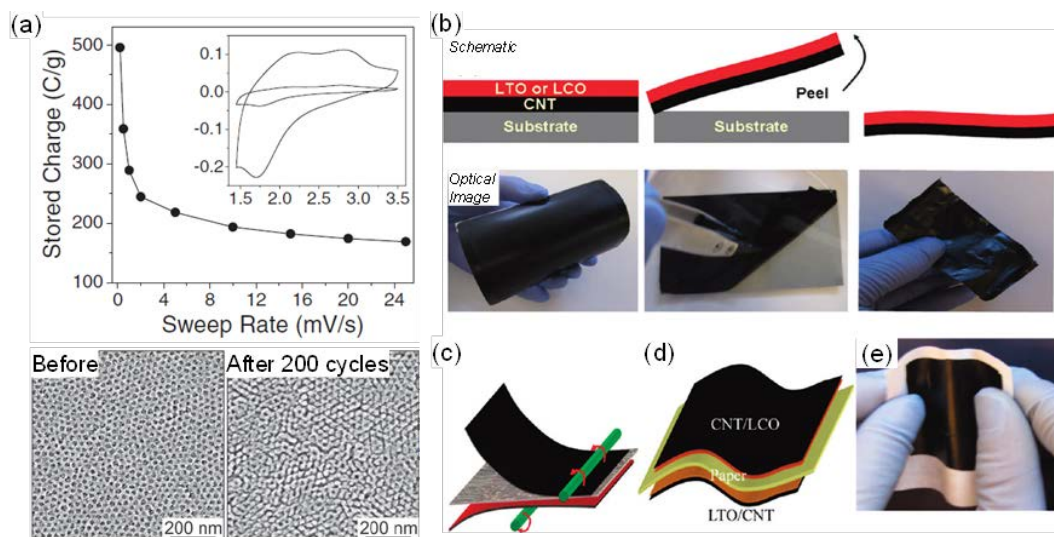


Figure 31. (a) Charging rates calculated from cyclic voltammetry at various sweep rates for  $\alpha\text{-Fe}_2\text{O}_3$  Li-ion battery electrodes. An associated cyclic voltammetry graph for two different sweep rates after 5 cycles is included in the inset. Reproduced with permission from ref 190.<sup>[190]</sup> (b) Fabrication schematic and corresponding optical images outlining the formation of a solution processed free standing LTO/LCO Li-ion electrode. (c) Lamination process where the free standing film is adhered to paper. (d) Schematic and (e) optical image of a Li-ion paper battery prepared from the free standing LTO/LCO Li-ion electrodes. (b-e) reproduced with permission from ref 62.<sup>[62]</sup>